EFFECT OF SPECIMEN GEOMETRY AND TEST CONFIGURATION ON THE FRACTURE PROCESS ZONE FOR ASPHALT MATERIALS

BY

JOSE J RIVERA-PEREZ

THESIS

Submitted in partial fulfillment of the requirements
for the degree of Master of Science in Civil Engineering
in the Graduate College of the
University of Illinois at Urbana-Champaign, 2017

Urbana, Illinois

Advisors:

Professor Imad L. Al-Qadi
Assistant Professor Hasan Ozer

ABSTRACT

In the United States and elsewhere in the world, recycled materials are commonly incorporated into asphalt mixtures, to provide environmental and economic benefits by decreasing the use of virgin materials, such as natural or quarried aggregates and asphalt binder, in newly designed asphalt mixtures. However, recycled materials such as reclaimed asphalt pavement (RAP) and recycled asphalt shingles (RAS) have resulted in asphalt mixtures prone to early cracking. In addition, Superpave volumetric design requirements are no longer sufficient to design asphalt mixtures because of the inconsistent properties of RAP or RAS. Consequently, agencies have been adopting performance tests to assess the cracking and rutting vulnerability of asphalt mixtures to achieve a balance mix design.

The Illinois Flexibility Index Test (I-FIT) protocol was developed at the Illinois Center for Transportation (ICT) and published as American Association of State Highway and Transportation Officials provisional standards (AASHTO TP 124) to evaluate the cracking vulnerability of asphalt concrete. The test consists of a semi-circular asphalt concrete sample that has a vertical notch loaded along the symmetric axis resulting in mode-I type of fracture similar to, the typical three-point bending beam tests. The I-FIT global response refers to the load-versus-displacement curve that is characterized using the fracture energy (FE), strength, and post-peak slope. The microstructural response refers to the deformation occurring in the fracture process zone (FPZ). FPZ is the region surrounding the notch tip that develops micro cracks before a macro crack is observed. Hence, the energy dissipation due to the deformation that occurs in this region eventually controls the global response of the specimen. I-FIT outputs are influenced by specimen geometry and test conditions (e.g., thickness, and loading rate, as well field aging). For this reason, there is

a need to understand the effect of test parameters on global and microstructural responses to calibrate the I-FIT results when test parameters are altered. Therefore, this work investigates the effect of the notch length, specimen thickness, loading rate, air void content, and asphalt binder on I-FIT global results and microstructural response. Multiple samples with varying notch lengths, thicknesses, and loading rates were evaluated to observe the effect of the test parameters. Then, samples with varying air void content and asphalt binder were tested to observe the mixture properties effect. The tests were recorded with high-resolution cameras to allow for digital image correlation (DIC) measurements. DIC measured the strain and displacement fields at a resolution of 8 microns/pixels. The resolution allows to evaluate the local characterization of fracture mechanisms and the interaction between the asphalt mastic and aggregate phases.

It was found that an increase in the thickness or loading rate resulted in an increase of the post-peak slope without affecting the FE. On the other hand, an increase in the notch length or air voids content resulted in lower post-peak slope values. The FE was affected by the notch length and the loading rate. From, DIC results, it was seen that a decrease in the FPZ area correlated to a decrease in the FE and lower post-peak slope. The results from varying the notch length did not follow this trend because, as the notch length gets longer, the compressive strain (not included in the FPZ definition) interacts as an energy dissipation mechanism at failure. It can be concluded that existing correction factors that address the variation due to specimen thickness and air void content are appropriate. A new correction factor to account for the notch length is proposed. Finally, the specimen properties affect the microstructural response of the specimen. As the one of the test parameter (thickness, notch length, loading rate, or air voids) is modified, the size of the FPZ changed.

To: Carmen Gloria Pérez Torrado (Mother) & Julio Rivera Reillo (Father)

& Carlos Rivera Pérez (Brother)

ACKNOWLEDGMENTS

First, I thank God for always being my refuge and strength, and the ever-present help throughout my career. I would also like to thank my adviser, Professor Imad Al-Qadi, who believed in me and gave me the opportunity to be part of his research group. His support and guidance are the cornerstone of my graduate studies at the University of Illinois.

I thank my co-adviser, Dr. Hasan Ozer, for sharing his knowledge and expertise throughout my graduate studies. Along with Dr. Al-Qadi, he has become a role model for me. I acknowledge the Illinois Center for Transportation and the Dwight David Eisenhower Transportation Fellowship Program for funding this study. Open Roads Paving and Jeff Kern for providing material for conducting this research effort. The work of the Research Engineers Jim Meister, Greg Renshaw, and Senior Mechanic Marc Killion who provided their laboratory technical expertise is sincerely appreciated. I particularly thank my colleagues Punit Singhvi, Berangere Doll, Jaime Hernandez, Issam Qamhia, Sushobhan Sen and the entire research team at UIUC for helping me through my graduate studies.

I would like to thank my family for their continued support, specially my parents, Julio Rivera and Carmen Perez, my brother Carlos, Gloria, Carmelo, Julio, Digna, Aby, Nilsa, Domingo, Monse and all my family that I couldn't list here. I could not have completed my studies at the Universities of Puerto Rico and Illinois without them! Finally, but most importantly, Puerto Rico and United States, both are my homeland and my inspiration. No matter how difficult our economic circumstances might be, we have demonstrated that we can overcome them by working together as one nation.

TABLE OF CONTENTS

CHAPTER 1 : INTRODUCTION

1.1 Background

The asphalt industry is a major recycler sector in the United States. According to the National Asphalt Pavement Association, over 90 % of asphalt pavements materials are recycled annually [1]. Reclaimed (or recycled) asphalt pavements (RAP) are typically incorporated into newly designed asphalt mixtures to reduce the consumption of virgin materials and pavement costs. As an example, in the United States, four million tons of fresh asphalt binder have been saved from 2009 to 2010 by increasing the RAP and RAS content to 60 % and 10%, respectively [1]. In 2014, 71.9 million tons of RAP were used in the United States, a 6 % increase over the tons used in the previous year. Meanwhile, in the State of Illinois, the recycled content in an average mile of construction increased four times between 2009 and 2013 [2].

The use of RAP helps to achieve sustainable pavements, but economic savings depend on the pavement capacity to perform similar (or better) to equivalent pavements that are free of recycled materials. Although RAP leads to a decrease in rutting at intermediate and high temperatures, it increases low-temperature cracking potential [3] [4] because of the aged binder which makes it stiffer. In addition, RAP stockpiles do not have consistent gradations, and the selection of a representative bulk specific gravity is difficult. Thus, the use of RAP makes it difficult to achieve the desired volumetric for mixtures. [5] Due to these challenges, Superpave volumetric requirements are not sufficient by itself for designing mixtures. Hence, there is a need for a cracking performance test, along with the Superpave Volumetric and the Hamburg wheel tracking device to design balance asphalt mixtures that can withstand both cracking and rutting during pavements design life.

In 2015, the Illinois Center for Transportation (ICT) published the report "Testing Protocols to Ensure Performance of High Asphalt Binder Replacement Mixes Using RAP and RAS," proposing a test methodology to evaluate the cracking performance of asphalt mixtures [5]. In the study, multiple fracture tests were evaluated to identify a method that can detect changes in cracking performance among mixes with variable recycled contents. In addition, the test needed to be economical and easily implementable so it could be adopted by the Illinois asphalt industry. The study proposed a modified version of the semi-circular bending beam (SCB) test to meet the requirements. The modified SCB test is run at a temperature of 25°C and a loading rate of 50 mm/min, thus allowing specimen testing without the need for an environmental chamber. The study found that FE was insufficient for discriminating cracking performance within the mixtures. The FE can be similar between asphalt mixtures showing different crack propagation [5]. To address this issue, the Flexibility Index (FI) was developed based on the total fracture resistance and post-failure crack propagation. The calculation of FI includes both FE and the slope at the inflection point of the post peak curve. [6]. The FE indicates the total resistance of the sample, while the slope denotes the crack propagation speed; a higher post-peak slope indicates a brittle crack propagation and vice versa. This parameter was shown to discriminate cracking performance within mixtures of variable recycled material contents [7]. The modified procedure was named the Illinois Flexibility Index Test (I-FIT) and accepted as American Association of State Highway and Transportation Officials (AASHTO) Provisional Standards TP 124.

A limitation of the I-FIT procedure is the dependency of the FI on the specimen and test characteristics [8]. When AC specimens fail to meet the standard specifications, this may result in misleading FI values. Although, laboratory-compacted specimens can be prepared to meet the I-FIT test requirements, field cores may not meet such requirements. For example, the field core

sample thickness depends on the AC layer where the core was extracted and might not satisfy the 50 mm requirement. Also, contractors might lack proper equipment needed for preparation of the notch, thus failing to meet the 15 mm length requirement. In addition to the geometric challenges, the field cores have variations in the air voids content that can affect the FI results [8]. Previous studies developed correction factors, such as the original I-FIT study [5] which proposed a thickness correction factor for the FI and Barry 2016 who proposed a correction factor for air voids variation [8]. These studies helped address the test dependence of the FI but other factors are yet to be considered.

In this study, five test and specimen properties are modified: thickness, notch length, air voids, binder type, and loading rate. The test dependence of the I-FIT results is investigated at the global response and microscale levels. At the global response level, the study considers the variation of the FI, post-peak slope, and FE. At the microscale level, the effect of the test properties to the area known as the fracture process zone (FPZ) is considered. The FPZ is the area close to the notch tip of the specimen where microcracks and energy dissipation occur prior to macrocrack propagation. The deformation that occurs within this region influences the pre-peak portion of the global load vs displacement curve wherefrom the FI is derived. Thus, the variation in the FI is related to the variation in the damage occurring in this region.

Previously, other studies used various measuring techniques such as acoustic emissions (AE) and digital image correlation (DIC) to detect the FPZ. In this study, DIC was selected to measure the opening strain field at the FPZ. DIC is a full-field measuring technique that has been implemented in asphalt concrete in previous studies [9] [10]. In this technique, a speckle pattern is painted over the surface of the I-FIT specimen. Then, successive images of the pattern are taken during the test. The pictures are compared with a reference image taken before the deformation to compute the in-

plane displacement and strains [11]. This technique has the advantage of being applied at intermediate and low temperatures (25^{o}C, -12^{o}C).

1.2 Problem Statement

Since its implementation, the I-FIT has proved effective and easy for identifying asphalt mixtures prone to crack. The results of the test correlate with the field performance of asphalt mixtures, detecting changes in mixtures stiffness. In addition, the relatively low cost of the fixture has made the test affordable to contractors and industry. But, like other fracture tests, the results are specimen-dependent, meaning that the specimen must be prepared and run in accordance with the AASHTO TP 124-16. Thus, failure to meet the specifications could lead to incorrect results. This problem occurs when field cores are used for I-FIT specimens and the thickness or the notch length does not meet the requirements due to fabrication limitations.

In the previous studies, dependency of I-FIT results with respect to thickness and air voids were investigated and correction factors were provided for both parameters [5] [8]. However, there is a lack of fundamental understanding of geometry dependence on the I-FIT results and whether these differences can be explained by the microstructure behavior. In addition, variations in the loading rate and notch length have not been studied at both scales: global and microstructural responses. Therefore, this study contributes to fill this gap in the literature and develop a FI correction method for the variation in the notch length. In addition, the thickness and air void content correction factors available in the literature are revised.

1.3 Objective and Scope of Research

This study aims to provide a better understanding of the specimen geometry dependence of the I-FIT results at the local and microstructure scale while focusing on the following objectives:

• Evaluate the effects of thickness, notch length, air voids, loading rate, and binder grade on the global response of the I-FIT (FI, post-peak slope, FE).

• Evaluate the effects of thickness, notch length, air voids, loading rate, and binder grade on the specimen microstructure by measuring the damage at the FPZ using DIC.

• Develop or select a correction factor for the non-standard thickness, notch length, and air void content that can adjust the results to the conditions specified by AASHTO TP 124-16.

To achieve these objectives, the Illinois Flexibility Index Test was conducted on specimens with various thicknesses, notch lengths, air voids, loading rates, and binder grades. These specimens were produced using laboratory-designed asphalt mixtures with controlled volumetric properties and no recycled content. DIC was used to measure the deformation and strain field in the region close to the notch tip to assess the effect of test parameters on the material during the fracture test. Using the strain threshold region, the area of the specimen where the FPZ occurs is identified and measured. This allows to relate the behavior at the microstructure with the global I-FIT results.

1.4 Research Impact

This study is aimed at understanding the impact of specimen geometry and test characteristic on the I-FIT results and to calibrate FI values according. Cracking prediction of AC using the recently developed I-FIT procedure was improved. This study improved the prediction of asphalt concrete potential cracking. A better understanding of AC fracture at the intermediate temperatures in the

microstructure scale was achieved. The accurate prediction of asphalt concrete pavement cracking allows proper planning for maintenance and rehabilitation and allocation of funds. Most importantly, optimizing the time of maintenance and rehabilitation based on the FI values can help in better fund allocation and reduce disturbance to mobility at work zone areas.

CHAPTER 2 : LITERATURE REVIEW

2.1 Fracture Characterization

Multiple tests can be found in the literature to evaluate fatigue and thermal cracking. To characterize the fatigue life of HMA at intermediate temperatures, the Texas overlay test (TOL), flexural beam fatigue test, and the push-pull test are commonly used. The TOL measures the AC reflective cracking resistance by applying cyclic displacements simulating the opening and closing of joints that initiate the crack [12] [13]. The flexural beam fatigue simulates the fatigue life of asphalt pavement under repeated traffic loading. A sinusoidal loading is applied using a 4-point loading fixture to the AC beam at a specified strain limit until failure [14]. The number of loading cycles to failure and the dissipated energy are used to evaluate the performance. Both TOL and flexural beam fatigue tests are conducted at intermediate temperature (25°C). The push-pull test determines the continuum damage characteristics of asphalt mixtures by subjecting a cylindrical pill of AC to uniaxial compression and tension. The test is based on continuum damage theories and is usually conducted at temperatures ranging from 15°C (59°F) to 20°C (68°F) at multiple microstrain levels [15].

Low-temperature cracking is commonly characterized using the single-edge notched beam (SENB) test, semi-circular bending (SCB), and disk-shaped compact tension (DCT). The SENB is used to evaluate the FE and toughness of the asphalt concrete (AC) mixtures. In this test, an AC beam specimen with a notch at the center is subjected to three-point bending. The test allows for mixed-mode fracture properties, but the difficulty of fabricating the specimen renders the test hard to be used in the field. Thus, practical tests such as the SCB and DCT were developed to consider the geometry of asphalt concrete pills and field cores. The DCT test uses a circular specimen with

a single-edge notch loaded in tension at low temperatures that allows field cores be tested [16]. The FE and the critical crack tip opening displacement can thus be measured. Although, the DCT allows for testing of circular geometries, the limitations of specimen preparation may pose challenges for contractors [5]. In addition, the end fixture may cause load eccentricity and the closed-loop CMOD control elevates the cost of the fixture [17]. The SCB test can address these issues by using a simplified test fixture and specimen geometry. It consists of a semi-circular AC with a notch at the center subjected to three-point bending, similar to the SENB [18]. In contrast to the SENB, the specimen geometry allows samples fabrication from field cores and laboratory-compacted asphalt pills. The FE and fracture toughness are evaluated from the load vs displacement curve recorded during the test. The test can be conducted at low and intermediate temperatures.

A modified version of the SCB test (known as I-FIT) was adopted with significant changes to the test procedure and data analysis. The I-FIT has multiple advantages over other tests. First, SCB specimen preparation is feasible for contractors, and the test can be conducted using a low-cost test fixture. In contrast to the FE, the FI allows for a significant spread of test results. Thus, mixtures with variable cracking performance could be detected. The results of the I-FIT correlated with other fatigue tests and field performance [6]. For example, the result of the I-FIT correlated with the cycles to failure of several AC lanes (with varying recycled content and additives) tested using the Accelerated Loading Facility of the FHWA in Virginia [6]. Also, the I-FIT results of field cores from multiple Illinois Department of Transportation (IDOT) districts correlated with their observed field performance. The study concluded that the I-FIT is a feasible and economical method for identifying field cracking performance.

2.2 Illinois Flexibility Index Test

The Illinois Flexibility Test is a modified version of the SCB test (AASHTO 105-13) that uses a semi-circular asphalt specimen subjected to three-point bending, as shown in Figure 2.1. The specimen has 50 mm thickness and 150 mm diameter with a 15 mm notch made at the center of the specimen [19].

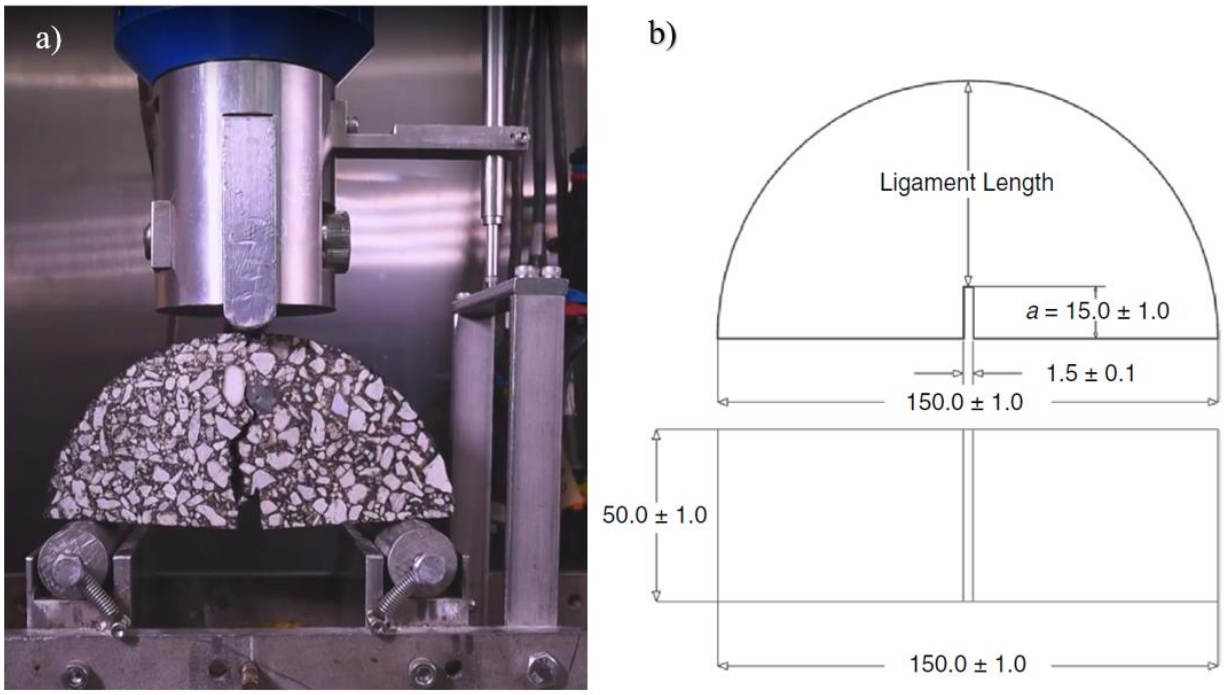

Figure 2.1: Illinois flexibility index test a) fixture b) specimen geometry

During the test, the specimen is placed over two rollers, with a monotonic load applied along the vertical diameter of the specimen at a displacement rate of 50 mm/min controlled by linear variable differential transformer (LVDT). From the load vs. displacement curve, the work of fracture and FE can be computed as follows [19]:

Work of Fracture:

$$W_f = \int_0^{u_f} P\, du \text{ (Joules)} \tag{2.1}$$

Fracture Energy:

$$G_f = \frac{W_f}{Crack\ ligament\ Area} X\ 10^6 \quad \left(\frac{Joules}{m^2}\right) \tag{2.2}$$

where P is the load, u the LVDT displacement, W_f is fracture energy, and G_f is the work of fracture.

The Flexibility Index (FI) is computed based on the fracture energy and slope of the post-peak load vs displacement curve as [19]:

Post Peak Slope:

$$m_{pp} = \frac{dP}{du}\ (at\ Post\ Peak\ Inflection\ Point) \tag{2.3}$$

FI:

$$FI = \frac{G_f}{m_{pp}} X\ A \tag{2.4}$$

where m is slope (kN/mm), and coefficient A is a unit conversion factor and scaling coefficient (taken as 0.01). The FE indicates the energy required to create a unit surface area of a crack, while the slope is an indication of the crack propagation speed; a higher post-peak slope indicates a faster (brittle) crack propagation and vice versa. As the FI increases, flexibility of the mixture increases and cracking vulnerability decreases. Currently, IDOT considers a FI of 8 to represent an acceptable AC mix.

2.3 Specimen Dependence of Fracture Tests

The Illinois Flexibility Index results (FE and FI) are not fundamental material properties because they could be affected by either specimen or test framework characteristics. Specimen and test dependency is common among fracture tests regardless of the material or the specimen geometry. For metals, Mussler et al. evaluated the fracture toughness dependence of alumina using a notched

beam. The results showed that the measured fracture toughness was sensitive to the notch radius [20]. Krager-Kocsis et al. studied thickness dependency by testing a ductile polymer using a double-edge notched specimen [21]. In the study, the authors analyzed the FE released by the process zone and the plastic zone separately (both components add up to the total FE) [21]. It was concluded that the FE at the process zone was independent of the specimen thickness, unlike the FE caused by the plastic zone. However, these results contrast with previous studies by Hashemi et al. wherein the FE of both (process zone and plastic zone) exhibited specimen dependence [22]. Although the studies provided contradictory results for the plastic zone energy, the thickness plays a significant role in determining the total FE of the test. Kusaka et al. tested the rate dependency of carbon-fiber/epoxy composite laminates; a split Hopkinson pressure bar was used to insert a wedge at the mouth of a double-cantilever beam specimen to produce pure Mode I fracture opening [23]. The study indicated that fracture toughness decreases with increasing loading rates. This reduction in toughness was related to the stability of the fracture opening [23].

The effect of the specimen size for quasi-brittle materials, such as Portland cement concrete (PCC), was modeled and tested by Bazant in several publications [24]. Bazant developed the size-effect model that determines the FE of large-scale specimens based on the results of laboratory scale specimens [25]. Later, additional publications from [26] [27] Bazant, Planas, Guinea, Elices and Carpinteri have fully explored the influence of specimen size on the fracture behavior of PCC. In a Bazant and Kazemi study, the size dependence of the FE in PCC was investigated. The study evaluated the RILEM method for measuring FE from a SENB specimen of PCC, finding that the FE increases with larger specimen size and indicating sensitivity of FE to the relative notch depth [28]. It can therefore be concluded from the literature that fracture test results are generally dependent on the specimen dimensions for multiple test configurations and materials.

2.4 Test Condition Dependence in Asphalt Concrete

The test conditions dependence has been previously studied using asphalt fracture tests. In this section, the influence of the loading rate, thickness, air voids, and notch length documented in the literature is discussed.

2.4.1 Loading Rate

Wagoner et al. evaluated the effect of loading rate on FE using the DCT. Three rates (10, 5, 1, 0.1 mm/min) were tested at three temperatures: -20, -10, and 0^{o}C [17]. The results indicated that FE decreases as the loading rate increases regardless of the tested temperature [17] [29]. For the SCB test, Im et al. 2013 and Kim and Aragão 2013 evaluated the SCB load rate dependence experimentally and by finite element models, respectively. Im et al observed that at low temperatures (-10^{o}C), the loading rate does not affect FE. At 0^{o}C, the FE decreased as the loading rate increased; however, at 30^{o}C, the trend was reversed [30]. Kim and Aragão 2013 modeled the SCB failure by implementing and calibrating the cohesive zone model into the ABAQUS finite element software. In the study, laboratory SCB samples were tested at 21^{O}C to calibrate the model. The results indicated that the cohesive zone FE is rate dependent, increasing as the loading rates become faster [31].

Nsengiyumva studied the effect of multiple test variables (loading rate, thickness, and notch length) to select a practical configuration of the SCB test that can lead to repeatable results [32]. Plant-collected mixtures were used to prepare SCB specimens at 4% air voids and tested at 10, 5, 1, 0.5, and 0.1 mm/min loading rates under a temperature of 21^{o}C. The results showed a stiffer response for faster rates, causing a larger peak load [32]. The FE increased as the loading rate increased at intermediate temperatures.

2.4.2 Thickness

The thickness effect for the SCB test was studied by Nsengiyumva at intermediate temperature (21^{O}C) [32]. Several specimens of 30, 40, and 50, and 60 mm were tested. The results indicated that the maximum load and the FE increased as the specimen became thicker [32].

Al-Qadi et al evaluated the thickness effect when the I-FIT was proposed; specimens with thicknesses varying from 25 mm to 62.5 mm were tested showing that the FI decreased with the increase in thickness [8]. A correction factor was proposed based on the test results:

$$FI_{50} = \frac{t}{50} X\ FI \tag{2.5}$$

where *t* is the specimen thickness and the FI is the flexibility index.

Barry evaluated the correction factor proposed by Al-Qadi et al [5]. In the study, two mixtures were collected from a local plant, a 4.75 mm NMAS leveling binder mix and 9.5 mm NMAS surface mix. The specimens were prepared with a thickness of 10, 20, 30, 40, 50, and 60 mm. A trend similar to that observed by Al-Qadi et al was found; the FI decreased at larger thicknesses [8]. The FE was not significantly influenced by the thickness, but the slope increased with larger specimen, thus resulting in a decrease in the FI. Barry's study corroborated the FI correction factor proposed by Al-Qadi and suggested that the factor corrects just the change in slope:

$$m_{50} = \frac{50}{t} X\ m \tag{2.6}$$

As a result, this corrected slope led to the same FI from the equation (2.5).

2.4.3 Air Voids

Braham et al. studied the effect of air voids by experimental testing using the DCT. Two mixtures were tested to the target air void of the Superpave specification (4 %) and the actual void content in the construction (7 %). The results indicated that the air voids content is not a significant factor affecting the low-temperature DCT fracture energy results [33]. In a subsequent study, Li et al.

evaluated the low-temperature FE using the SCB and DCT tests. One mixture compacted at 4 % and 7 % air void contents, respectively, was considered. The results indicated the DCT fracture energy is not influenced by the air voids. However, the air void significantly influenced the SCB fracture energy [34].

Barry studied the impact of the air void content on the I-FIT results [8]. In the study, two mixtures were collected from a local plant, a 4.75 mm Nominal Maximum Aggregate Size (NMAS) leveling binder mix and 9.5 mm NMAS AC surface mix. The two AC mixes were compacted at an air void range from 3 % to 10 %. The results indicated a reduction in the peak load, FE, and post-peak slope with increased air void content [8]. The decrease in FE was the least significant. Based on the results, Barry proposed a correction factor for the FE, post-peak slope, and FI (the FI correction factor is the combination of the FE and slope correction factors) [8]:

Correction factor for fracture energy (G_f):

$$G_{fAV_{corrected}} = G_f * \frac{0.93}{1-AV} \tag{2.7}$$

Correction factor for post-peak slope (m):

$$m_{AV_{corrected}} = m * \frac{AV}{0.07} \tag{2.8}$$

Correction factor for Flexibility Index (FI):

$$FI_{AV_{corrected}} = FI * \frac{0.0651}{AV-AV^2} \tag{2.9}$$

where AV is the air void content as a decimal.

2.4.4 Diameter and Notch Length

Zegeye et al. studied the specimen size effect by using the SCB test with varying specimen sizes (76.4, 101, 147, and 296 mm diameter) and a constant thickness (31 mm) [35]. Three notch length ratios (notch length over radius) were tested. The samples were prepared from a plant-collected mix and compacted into slabs where the specimens can be cored. The results indicated that the

nominal strength decreases as the diameter or notch increases [35]. In addition, large-diameter specimens without a notch were tested and the failure occurred at the support and not in the center of the SCB [35]. In a study by Zhong et al, the energy release rate, peak load (kN), vertical displacement at peak load and strain energy to failure were compared for SCB specimens with varying notch lengths, however, no significant trend was found [36]. Finally, Nsengiyumva tested SCB specimens with notch lengths of 5, 15, 25 and 40 mm at intermediate temperatures ($21^{O}C$) while keeping the thickness constant at 50 mm [32]. The results indicated that with increased notch lengths, the maximum load and the FE decreased [32].

2.5 Fracture Process Zone of Asphalt Concrete

2.5.1 Introduction

In fracture tests, where a notch induces stress concentration, the fracture process zone is the region close to the notch tip where the material is deforming before a full crack is developed [37]. This deformation is often attributed to the development of micro cracks in the region. In the I-FIT, the fracture process zone is developed close to the notch tip during the pre-peak load portion of the test, commonly between aggregates in the binder-fine particle matrix. Deformation in this region influences the energy dissipation (FE) recorded in the I-FIT. The FPZ size is a key factor to select the geometry and size of fracture test specimens. In addition, the parameter has been used in previous studies to calibrate numerical simulations based on the cohesive zone model [38]. Therefore, the experimental evaluation of this zone allows to characterize the microstructure behavior.

2.5.2 Fracture Process Zone Identification and Measurement

To detect the location and extent of the fracture process zone, a measuring technique that allows for local material characterization is required. Traditionally, the measurement of stresses and

strains in an AC test has been done using strain gauges, or test fixture sensors (linear vertical displacement transducer, crack mouth opening displacement, or load sensors). Strain gauges provide localized measurements that cannot characterize the full extent of the FPZ. Thus, acoustic emissions and DIC have been implemented to identify the fracture process zone in AC fracture tests.

Acoustic Emission (AE) Tests have been used to study the microstructure and fracture process zone in rocks [39], PCC [40], and AC [38]. An AE refers to the release of energy through a stress wave when the material is deformed [41]. The micro cracks within the fracture process zone generate an acoustic emission. Previous studies on the FPZ used sensors to detect the location where the acoustic emission and the AE energy were generated. Otsuka and Date noted that AE events that add up to 95 % of the total AE energy released by the material before the peak load are associated with the FPZ in Portland cement concrete samples [40]. Li and Marasteanu applied the same definition for the FPZ in AC at low temperatures (-10^{O}C) [38]. Acoustic emissions are typically used in low-temperature AC tests because the mixture needs to be stiff enough to generate an AE event. At intermediate temperatures, asphalt viscosity makes it difficult to detect an AE. Thus, this technique cannot be used with the I-FIT.

Digital image correlation is an imaging technique that allows measurement of the full-field 2-D displacement and strain field over the surface of the specimen [11]. Before testing, the specimen surface is painted to produce a grayscale pattern. An image acquisition system captures images of the speckle pattern before and after it deforms. Each image is then meshed into subset units containing a unique grayscale pattern distribution. Finally, an image process software compares both images by using a matching algorithm that can establish correspondence between the subset greyscale patterns. The procedures assume that each point on the light intensity distribution is

constant throughout the test and that the subset deformation is homogeneous in-plane deformation. Light uniformity is achieved using two white lamps. Once the correlation is achieved, the displacement and deformation of the subset with respect to the original image are computed based on the following equations: [42] [43]

$$x' = x + u + \frac{\partial u}{\partial x}\Delta x + \frac{\partial u}{\partial y}\Delta y, \tag{2.10}$$

$$y' = y + v + \frac{\partial v}{\partial x}\Delta x + \frac{\partial v}{\partial y}\Delta y, \tag{2.11}$$

where *x* and *y* are Cartesian position coordinates, *u* and *v* are the *x* and *y* represent the displacements, and ‘ indicates the variables in the deformed state.

The FPZ is identified using the strain field measured from DIC. Previous studies compared the FPZ of multiple AC mixtures by defining a strain threshold. The zone in the specimen surface where the threshold is exceeded is defined as the FPZ. This approach was developed by Wu et al. (2011) where the tensile strain capacity was selected to measure the FPZ in PCC [44]. For AC, selecting a tensile strain capacity can be challenging because it would depend on the viscoelastic properties of the binder and the test conditions (temperature, loading rate, among other factors). As a result, previous studies have selected strain thresholds based on the literature. Although, the strain threshold value may not accurately define the exact boundary of the FPZ, the threshold can be used to compare the AC mixes because it is kept constant at similar test conditions.

For example, Doll selected strains higher than 3000 με as the FPZ at intermediate temperatures (25°C) and higher than 1500 με at low temperatures (-12°C) [45]. The 3000 με was selected in the range of the creep intercept values for AC at 60°C, as presented by Zelelew and Papagiannakis [46]. Hill and Buttlar selected a tensile strain between 100 με up to 2000 με for -12°C. The 100 με

was selected based on a previous study that determined that AC behaved linearly at this strain level [47]. The low-temperature threshold (1500 με) selected by Doll agrees with the range later selected by Hill and Buttlar.

Romeo determined tensile failure strain limits in stress-strain curve using DIC and un-notched SCB samples at 10^{O}C [48]. The SCB samples were loaded, and the DIC was used to measure the strain at the location where the initial macro crack in the SCB is developed. Then the stress vs DIC strain curve was plotted, and the moment when the fracture occurred was identified. The results indicated that the tensile failure limits range over 1500 to 3000 με for AC mixtures at 10^{O}C. These results are in the range of the tensile strain threshold results selected by Doll [45]. Therefore, in this study, the DIC technique was selected to identify and measure the size of the FPZ using the strain threshold approach based on the previously defined range by Doll for intermediate temperatures. The 3000 με threshold is used to identify the relative extend of the FPZ.

2.5.3 Effect of Specimen and Test Properties to the Fracture Process Zone

Previous studies have examined the effect of material properties on the size and shape of the FPZ. Zietlow and Labuz studied the size of the FPZ of four different types of rocks with variable grain size using three-point bending beam configuration and AE [39]. It was found that the FPZ size was not affected by the specimen size. In addition, the width of the process zone had a linear relationship with respect to the rock grain size [39]. Otsuka and Date used AE and X-rays to evaluate the FPZ in concrete by measuring its width and length. The results indicate that as the maximum aggregate size increases, the width of the FPZ increases and the length of the FPZ decreases [40]. Li and Marasteanu investigated the effect of temperature, aggregate, notch length, loading rate, asphalt content, and air voids on the FPZ using the AE approach by Otsuka and Date [40]. Their results are summarized in Table 2.1: [38]

Table 2.1: FPZ size variation (after Li and Marasteanu)

Factor	Tested Condition	As the Factor Increases	
		Width	Length
Temperature	-6, -18, -30°C	No Change	Decreases
Notch Length	5, 15, 30 mm	n/a	Decreases
Loading Rate	0.005, 0.0005, 0.00015 mm/min (CMOD)	No Change	No Change
Asphalt Content	Optimum Binder, Optimum Binder + 0.5%	No Change	No Change
Air Voids Content	4 %, 7 %	Increases	Increases
Mixture Aggregate	Limestone vs Granite	The width of the FPZ is larger for limestone	

Doll et al. evaluated the effect of temperature and recycled content on the FPZ using DIC and the SCB test. In the study, laboratory-designed AC mixtures with variable recycled content were designed and tested at -12°C, and 25°C, respectively. The results indicated that at lower temperatures or increased recycled content, the size of the FPZ decreases [45]. This corresponds to an increase in the brittleness of the AC mixture. In addition, the DIC technique could show that the FPZ is developed around the aggregates in the matrix of the mixture [45].

2.6 Summary

Based on the literature review, the following trends are expected for the fracture energy measured from the I-FIT samples:

- Loading Rate: faster rates cause an increase of the AC stiffness resulting in higher maximum load and fracture energy [32].

- Thickness: As the thickness increases the maximum load that the specimen resist is higher however, the strength and the FE remains similar [5].
- Air Voids: Due to increased damage at higher air void content, the FE slightly decreases as the air void content increases [8].
- Notch Length: As the SCB notch length increases, the specimen peak load decreases, resulting in a reduced FE. [32].

At the microscale, it is expected that the FPZ measured using DIC should reflect a decrease of size when the AC stiffness is increased due to mix properties (binder stiffness) or faster loading rate. When the specimen exhibits more damage and compliance (increased air voids) the FPZ size should increase [38]. Finally, the FPZ size decreases as the notch length increases for SCB [38].

CHAPTER 3 : METHODOLOGY

3.1 Asphalt Materials

Two control AC mixtures produced and designed in Advanced Transportation Research and Engineering Laboratory (ATREL) of the University of Illinois at Urbana-Champaign were used in this study. In contrast to plant produced AC mixtures, laboratory designed AC allows strict control of the volumetric properties. The mix design target was 4 % air voids at 90 gyrations. Both mixtures had the same volumetric properties but different binder grades (PG 70-22 and PG 64-22). The mixtures were designed using local aggregates: dolomite, crushed dolomite, natural sand, and mineral filler. Figure 3.1 shows the AC mix gradation:

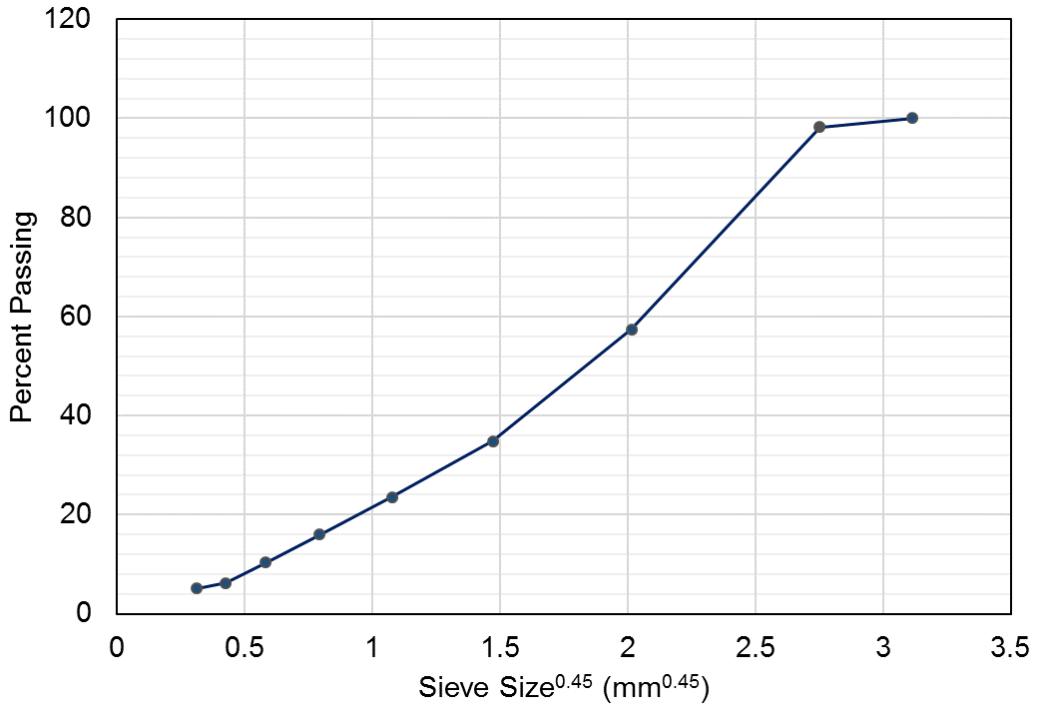

Figure 3.1: Control AC mixture gradation (for two mixes)

The gradation resulted in the volumetric properties shown in Table 3.1 for two mixes.

Table 3.1: Control mix volumetric properties

ID:	Mix 1	Mix 2
Binder	PG 64-22	PG 70-22 SBS
Binder Content	6.0 %	6.0 %
Bulk Specific Gravity at 90 Gyrations	2.394	2.392
Voids in Total Mixture	3.9 %	4.1 %
Voids in Mineral Aggregate	15.2 %	15.3 %
Dust Proportion	0.85	0.85
Voids Filled with Asphalt	74.40 %	72.80 %
Effective Specific Gravity	2.739	2.745
Absorbed Asphalt	1.20 %	1.29 %
Effective Asphalt	4.87%	4.79 %
Mixing Temperature	155^{o}C	160^{o}C
Compacting Temperature	147^{o}C	153^{o}C

I-FIT samples were prepared from the cylindrical pills of the laboratory-designed AC mixtures. The pills were compacted using a Superpave gyratory compactor at 7.0 % air voids. The 7.0 % air void content represents the targeted value during construction. The cylindrical samples of 150 mm diameter and 180 mm height were cut into semi-circular samples as shown in Figure 3.2. When the pills were cut, the top and bottom surfaces of the pill were removed, and two circular slices (50 mm thickness) were cut from the middle portion of the pill, as shown in Figure 3.2.

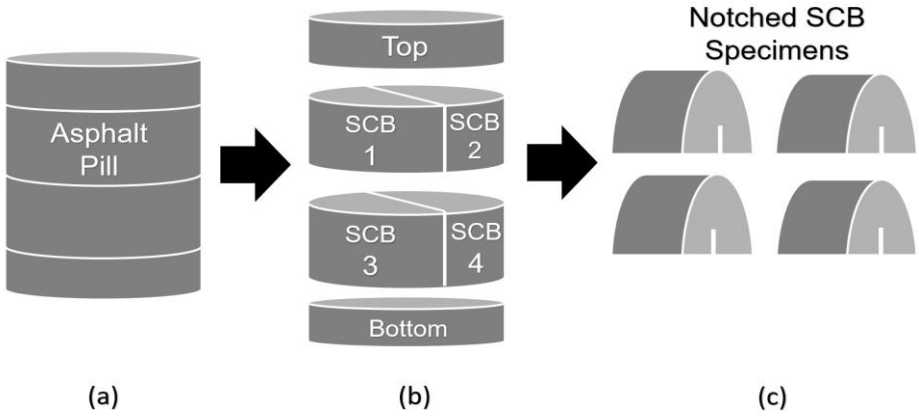

Figure 3.2: SCB preparation, a) 180 mm height compacted AC pill; b) pill is sawed into four semicircular samples; and c) a 15 mm notch at the center of the sample

Finally, the circular slides were divided into two semi-circular specimens and a 15 mm notch (15 mm length 2 mm width) was carved in the middle. As a result, the typical SCB samples had a 50 mm thickness, 15 mm notch length, and 7 % air voids. Then, depending on the parameter to be studied, properties of the specimen and the test were modified according to Table 3.2:

Table 3.2: Summary of conducted tests

Tested Parameter	Test No.	Replicates	Thickness (mm)	Air Voids (%)	Loading Rate (mm/min)	Notch Length (mm)	Binder Grade
Thickness	1	3	25	7	50	15	PG 64-22
	2	3	30				
	3	3	40				
	4	3	45				
	5	3	50				
	6	3	60				
Air Voids (VTM)	7	3	50	2	50	15	PG 64-22
	8	3		4			
	9	3		6			
	10	3		8			
	11	3		10			
Loading Rate	12	3	50	7	0.7	15	PG 64-22
	13	3			6.25		
	14	3			25		
	15	3			50		
Notch Length	16	3	50	7	50	10	PG 64-22
	17	3				15	
	18	3				20	
	19	3				35	
Binder Grade	20	6	50	7	50	15	PG 64-22
	21	6					PG 70-22

The AC mixture with PG 70-22 was used only to study the effect of binder grade. The study of the thickness, loading rate, notch length, and air void content used only the PG 64-22 as the binder.

3.2 Experimental Set-up

The I-FIT was conducted according to the AASHTO TP 124-16 using an Interlaken Technology Corporation (ITS) load frame. The specimens were conditioned using an

environmental chamber at 25ºC. A dummy specimen with a temperature gauge inserted into the center of the specimen was used to track the internal sample temperatures. After reaching 25ºC, the specimens were positioned over two rollers as shown in Figure 3.3.

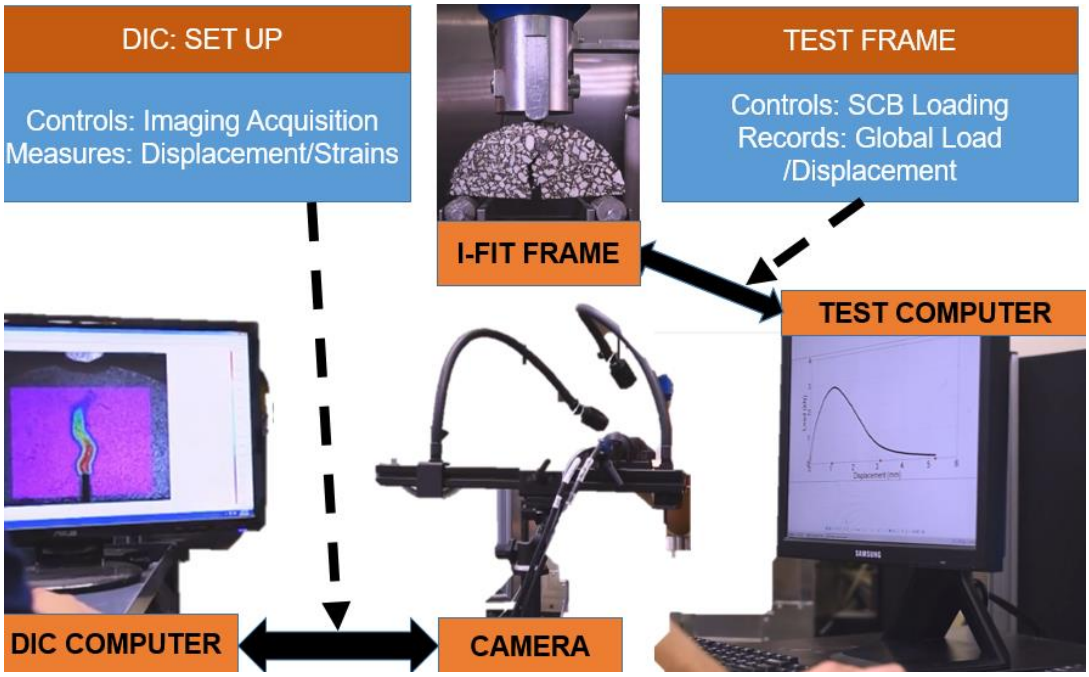

Figure 3.3: Experimental set up, on the left, a computer with the Vic2D software records images of the I-FIT surface; on the right, a test frame computer controls the I-FIT test loading and measures the applied load and displacement

The two roller supports were located 120 mm apart. Then, the load was applied along the vertical radius of the specimen load-line displacement (LLD) controlled using a fixed displacement rate of 50 mm/min, unless otherwise noted. The load and displacement data was recorded by the UniTest software provided by the load frame. The I-FIT data analysis was conducted using the I-FIT tool [49] developed by the ICT, which allows computation of FE, post-peak slope, I-FIT strength, and FI from the load vs displacement curve.

During the test, CCD (Charge Couple Device) camera captured images of the specimen surface. An Allied Vision Prosilica GX6600 was used with a Tokina AT-X Pro Macro 100 2.8D

lens. The set-up provided an image resolution of 29 Megapixel (6576 x 4384 pixels) at a speed of four fps. The camera was kept in a fixed location using a tripod and connected to a computer. It was controlled using the VicSnap (from Correlated Solutions Inc.) software which captured and saved the images. After the test is completed, the Vic2D software (from Correlated Solutions Inc.) was used to correlate the images, computing the displacement, and e_{xx}, e_{yy}, e_{xy} over the surface of the specimen.

3.3 Statistical Analysis

An analysis of variance test (ANOVA) was used to determine the statistical significance of the results found in this study. Typically, the results of our tests showed that the dependent variable remained constant or variated linearly with respect to the independent variable. Therefore, two analyses were conducted to determine if the trends were statistically significant. For the results that showed no variation, a one-way ANOVA analysis was conducted using IBM SPSS Statistic 22 to compute the p-value. The results are not statistically different if the p-value is larger than 0.05. For results that showed a linear variation, a regression was fit using Excel 2016 to perform an F-Test. Then, the coefficient of determination (r-square) and the significance F (probability that the regression does not fit the data) was computed. If the significant F value is lower than 0.1, the results fits to a linear regression trend.

3.4 Summary

A total of sixty-nine I-FIT were conducted variating the thickness, loading rate, notch length, binder and air void content. Images of the specimen surface were captured on each test using an Allied Vision Prosilica GX6600. Then the images were correlated and post processed to compute the strain field and FPZ. Finally, a statistical analysis was done to our results to determine if there

is a significant variation of the FE, slope, strength and FI a with respect to the test characteristics. If the FE, slope, strength and FI has a p-value larger than 0.05 from the one-way ANOVA analysis it is concluded that the parameter does not statically varied with respect to the independent variable (thickness, air voids, notch length, binder and loading rate).

CHAPTER 4 : I-FIT EVALUATION

4.1 Thickness Impact Evaluation

Twenty-Eight I-FIT specimens were prepared with target thicknesses of 25, 30, 40, 45, 50, and 60 mm, respectively, to evaluate the thickness impact on the FI. Figure 4.1 presents the load vs displacement curves of representative specimens. The peak load, post peak slope and the area under the curve (work of fracture) increased as the thickness increased. As a result, additional work of fracture was needed to break the fracture area where the crack propagated when the thickness increased. However, as the thickness increased, the specimen appeared to be less compliant in the pre-peak portion of the load vs displacement curve.

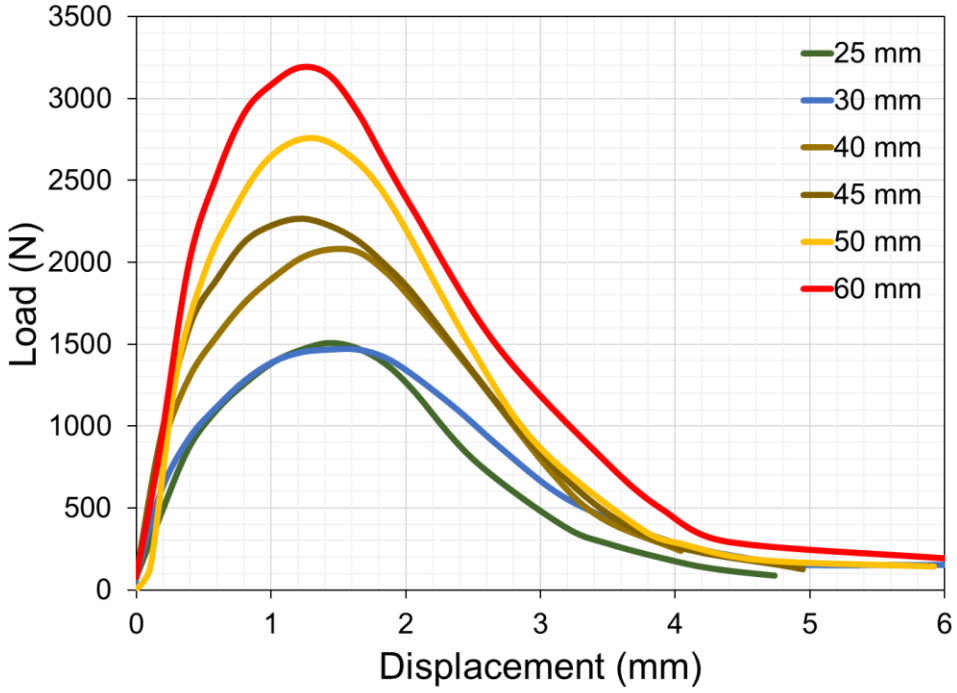

Figure 4.1: Load vs displacement curves for representative specimens of the thickness impact evaluation

The average I-FIT results are shown in Figure 4.2. It was expected that the FE increases with larger thicknesses due to the higher confining stresses at the crack fronts [8]. However, the results did

not indicate a significant change in FE. Using the average values shown in Figure 4.2-a, a one-way ANOVA analysis resulted in a p-value of 0.54, indicating that there is no significant variation in FE. Combining results from the six thicknesses, an average FE of 2301 J/m^2 with a standard deviation of 196 J/m^2 and a coefficient of variation (COV) of 8.5 % were computed. The COV value is within the acceptable range. The strength was not affected by the change of thicknesses; statistical analysis using the values from Figure 4.2-b resulted in a p-value of 0.27 (no significant variation). Combining the results from specimens with seven different thicknesses, the average strength was 355.7 kPa with a standard deviation of 32.4 kPa and a COV of 9.2. The results agree with the work report by Al-Qadi and coworkers (2015) and Barry et al. (2016). This suggest that no need for a correction factor the strength obtained at different specimen's thicknesses. On the other hand, the post-peak slope increased linearly with the increased thickness, resulting in a decrease in the FI, as shown in Figure 4.2-c-d. Statistical analysis suggested that the slope and the FI fitted a linear regression relationship with an R-square of 0.901 and 0.800, respectively. The F values are 3.1 x 10^{-7} and 1.8 x 10^{-7} for the slope and FI, respectively. Hence, a correction factor for the slope is needed when the specimen thickness varies from that of the specification.

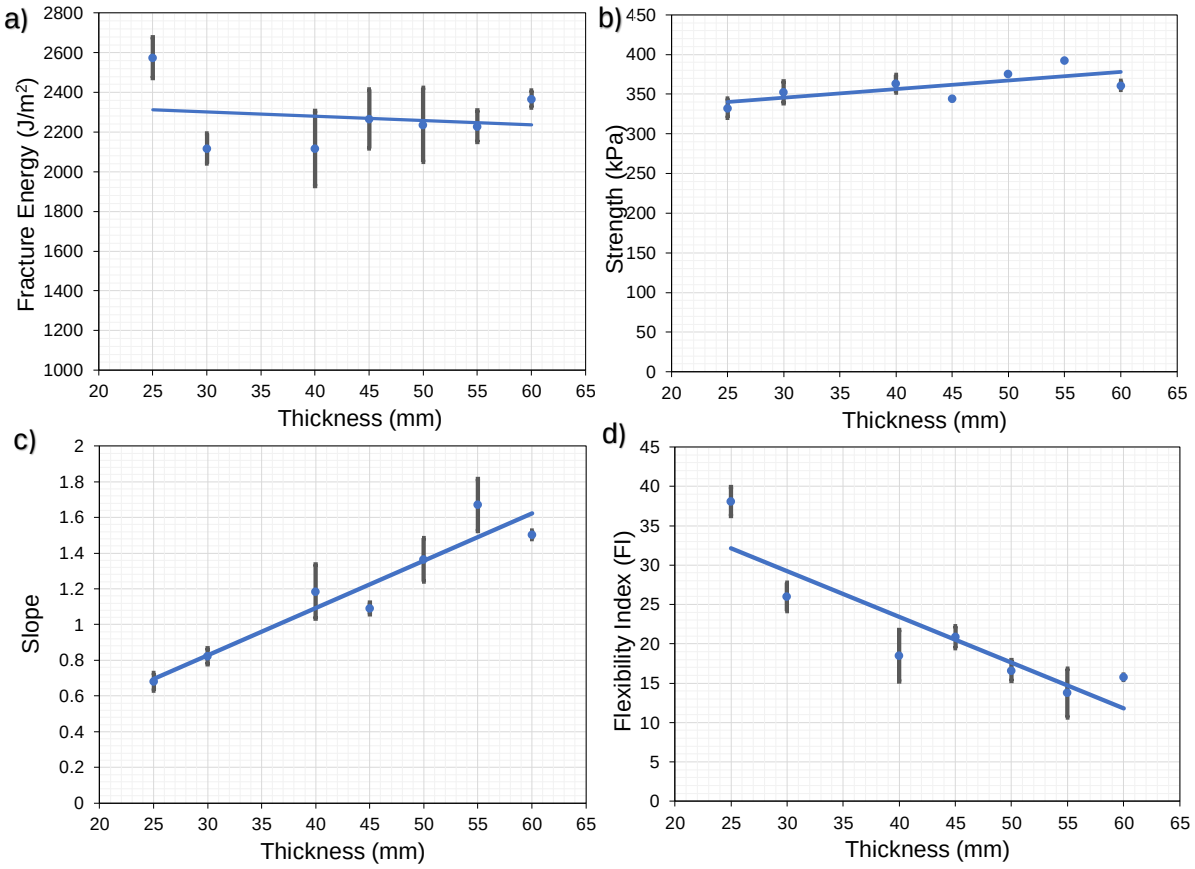

Figure 4.2: I-FIT results for the thickness impact evaluation: a) FE, b) strength, c) slope and d) FI

The correction factor for the slope (equation 2.6) as presented by Al-Qadi et al. (2015) was adopted as presented in Figure 4.3-a. The one-way ANOVA analysis of the corrected slopes resulted in a p-value of 0.57. Therefore, the variation in slope was corrected. The average corrected post-peak slope was 1.32 (considering the results from the various thicknesses) with a standard deviation of 0.16 and a COV of 12.2 %, respectively. The calculated corrected FI=17.1 is shown in Figure 4.3-b led to a FI 17.1 (standard deviation: 2.9 and COV: 16.5). The p-value for the corrected FI was 0.47 and, therefore, the correction factor from the literature can effectively address the variation in thickness.

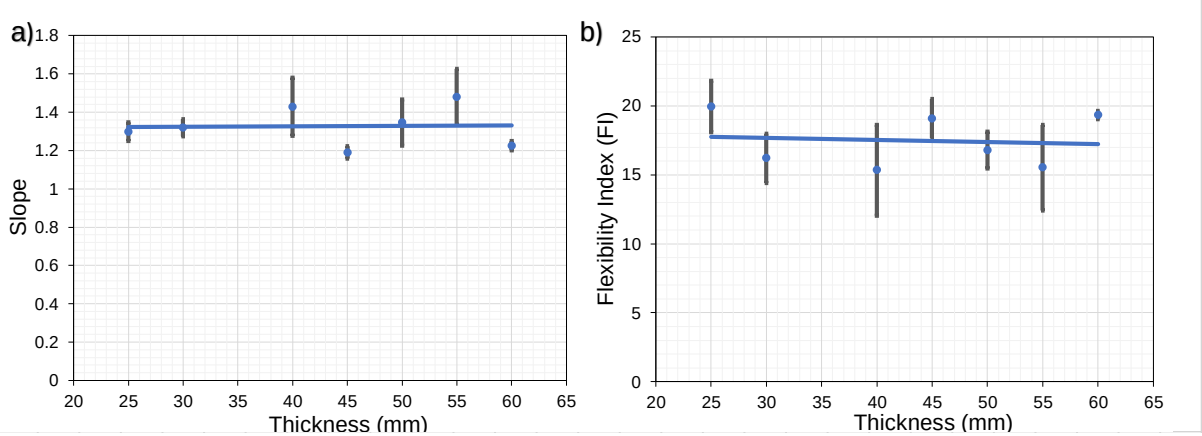

Figure 4.3: Thickness corrected results: slope (a) and FI (b)

4.2 Impact of Air Void Content of I-FIT Parameters

Twenty I-FIT specimens of Mix 1 were prepared with target air voids of 2, 4, 6, 8, and 10 % (voids in total mixture, or VTM). Volumetrics were measured for each specimen to determine the air void content. Typically, the specimens are tested within a week from sawing, but some specimens, due to schedule changes, remained on the shelf for a month and a half after sawing. Therefore, the final corrected FI (regarding air void) differs from other sections of the study. However, the specimens were prepared and tested under the same conditions to allow for a comparison of the air void content. Figure 4.4 shows the load vs displacement curve for several representative specimens. As the air void content increases, both peak load and post-peak slope decrease. This is due to the increased damage induced by the specimen's air void content.

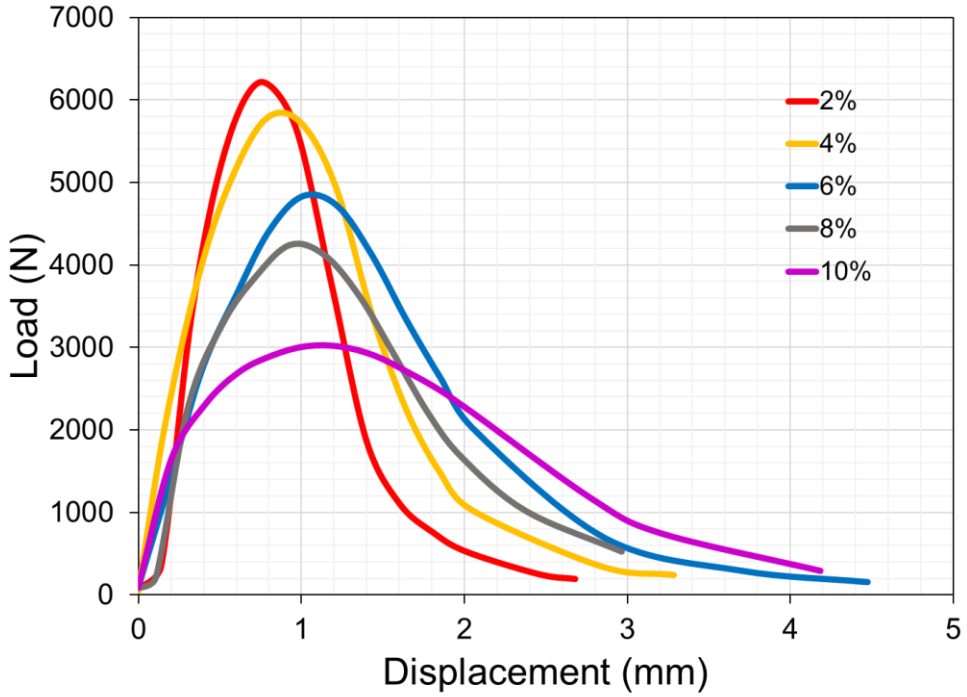

Figure 4.4: Load vs displacement curves for representative samples at different air void content

The I-FIT analysis results are shown in Figure 4.5. Initially, it seemed that the FE slightly increased with the increase in the air void content. However, the one-way ANOVA statistical analysis resulted in a p-value of 0.486; suggesting that FE did not statistically vary with respect to air void content. The average FE is 2258 J/m^2 and the standard deviation is 218 J/m^2. This results in a COV of 9.7 %, which is within the acceptable ranges for FE.

The strength and post-peak slope linearly decreased as the air void content increased. A linear regression was fit to slope values versus specimen's air void content, resulting in a significant F value of 4.11 x 10^{-8} (a significant F value lower than 0.1 results in an accepted fit). Therefore, the slope decreased, resulting in an increase in the FI. As shown in Figure 4.5-d, the FI linearly increased until 8 % air voids. The results for 10 % air void content, which is extremely high, were considerably off the linear trend due to the high plasticity and damage experienced at this level. There is also a notable difference in the load-displacement curves with the 10 % air void

specimens. As a result, all values up to 8 % air voids were considered of the correction factor for air voids.

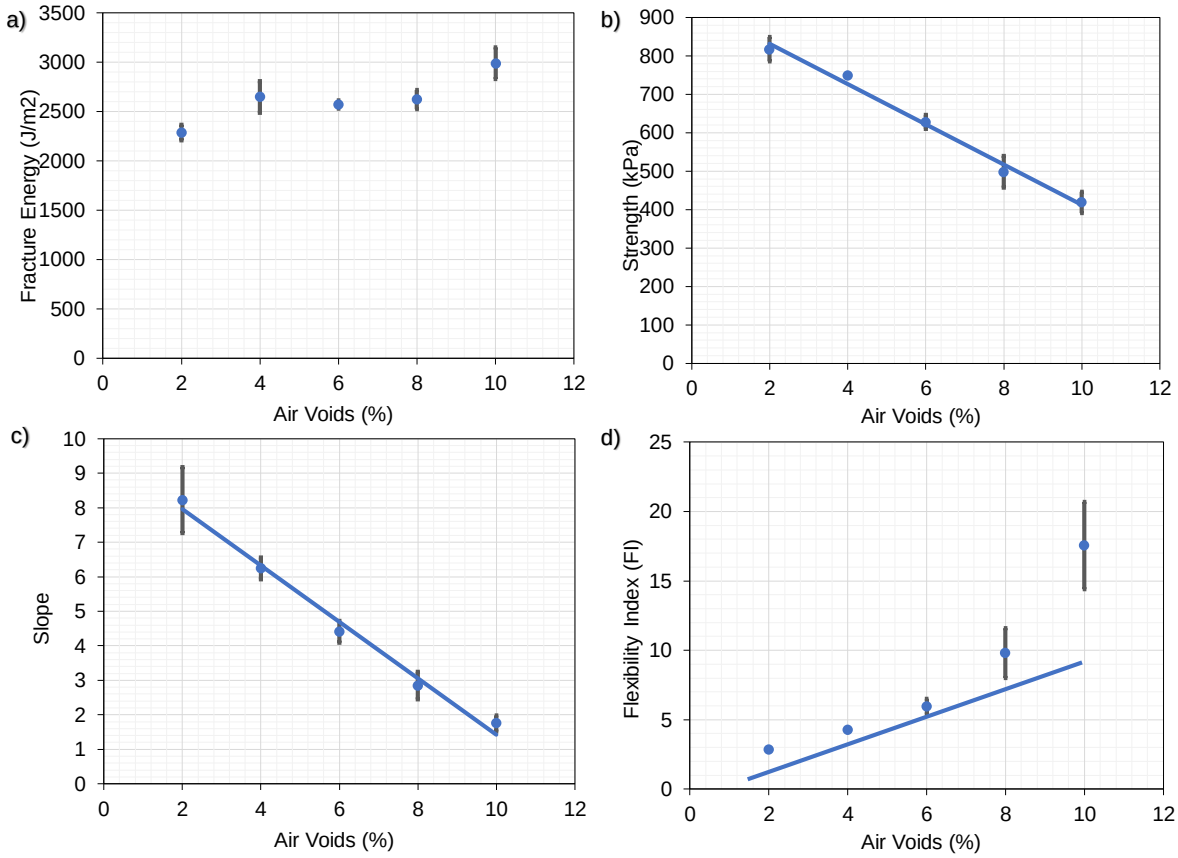

Figure 4.5: Air void content impact on I-FIT results: a) FE, b) strength, c) slope and d) FI

The correction factors proposed by Barry (2016), were used to correct for the air void content variation, Figure 4.6. Results indicate that the correction factor for the FE did not have a significant impact; the corrected and uncorrected FE values are similar, Figure 4.5. On the other hand, the slope was corrected using Barry et al. (2015) approach. The average corrected slope is 2.82 with a standard deviation of 0.59 and 21 % COV, respectively. Consequently, the average FI becomes 9.52 with a standard deviation of 2.25 and 23.6 % COV, respectively. The ANOVA analysis indicates a p-value of 0.588 and 0.081 for the slope and the FI, respectively (p-value > 0.05 results in successful correction). It was concluded that the air voids correction factor for the slope

proposed by Barry et al. (2016) could address the variation in the FI without the need of correcting the FE.

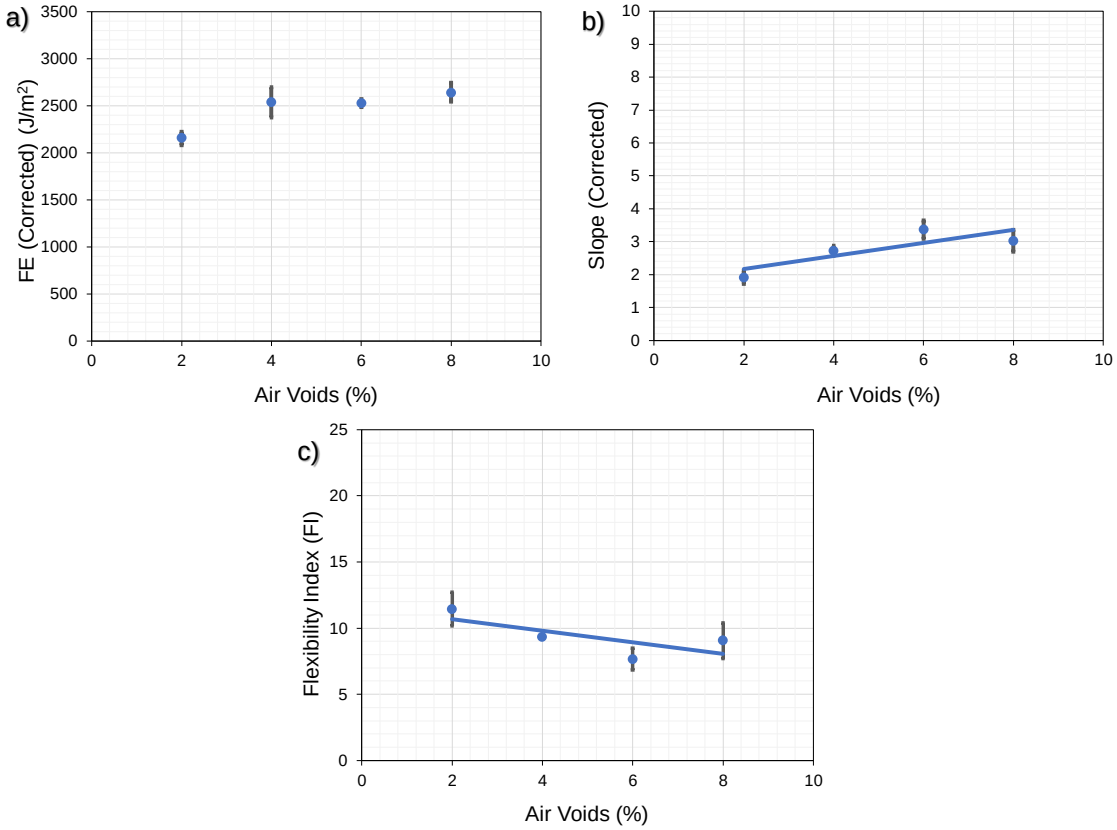

Figure 4.6: Air voids corrected a) FE, b) slope and c) FI

4.3 Effect of Notch Length on I-FIT Parameters

Sixteen I-FIT specimens with notch lengths of 10, 15, 20, and 35 mm were prepared from Mix 1 to evaluate the impact of the notch length. Figure 4.7 shows the load vs displacement curves of representative specimens for each notch length. A decrease in the peak load, post-peak slope, and the area under the load vs displacement curve (work of fracture) was observed when the notch length increases. The peak load and the work of fracture decreased because of the reduction in the ligament area (less work of fracture is needed to fracture a smaller area).

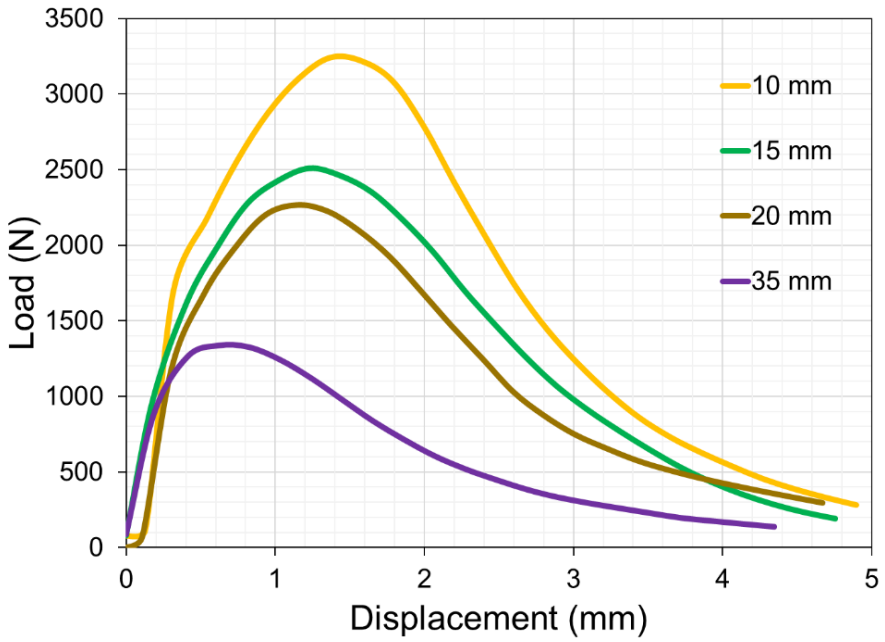

Figure 4.7: Load vs displacement curves for representatives specimens of different notch lengths

Figure 4.8 shows the results for FE, strength, slope and FI. As would be expected FE and strength did not remain constant due to normalization by the ligament area; the values decreased linearly with notch-length increase. The results from the ANOVA analysis indicate a significant linear trend as shown in Table 4.1.

Table 4.1: ANOVA analysis results for the effect of notch length on I-FIT parameters (*linear relation)

Parameter	R-Square*	Significance F
FE	0.76736	0.00290
Strength	0.64061	0.00542
Slope	0.61304	0.00740

On the other hand, the one-way ANOVA analysis for FI resulted in a p-value of 0.03. Thus, the FI did not demonstrate any significant variation with respect to the change of notch-length because the reduction in the FE and slope compensated for such variation. However, a correction for the FE and slope is recommended.

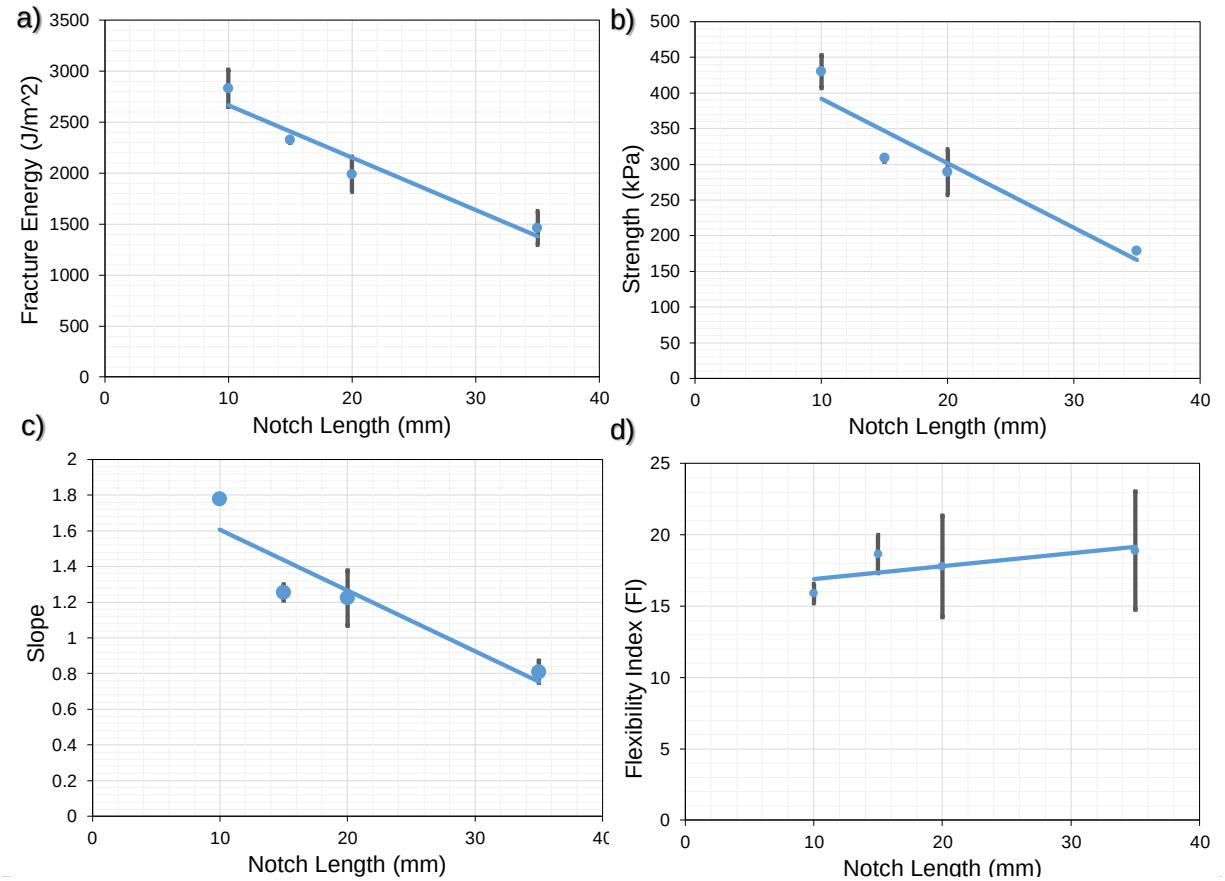

Figure 4.8: I-FIT results for the notch length evaluation: a) FE, b) strength, c) slope and d) FI

The FE and slope are linearly normalizing to the 15 mm notch length. The correction factors are presented in Equations 4.1 and 4.2:

Correction factor for fracture energy (G_f):

$$G_{fNL_{corrected}} = G_f * \frac{Notch\ Length\ (mm)}{15} \tag{4.1}$$

Correction factor for post-peak slope (m):

$$m_{NL_{corrected}} = m * \frac{Notch\ Length\ (mm)}{15} \tag{4.2}$$

Equations 4.1 and 4.2 were applied to the results as shown in Figure 4.9. The average FE is 2062 J/m^2 with a standard deviation of 255 and 12 % COV, respectively. The average slope is 1.36 with a standard deviation of 0.37 and 28 % COV. Consequently, the average FI led to 15.6, a standard

deviation of 2.86 and 18 % COV. A one-way ANOVA analysis was run to the corrected FE, slope, and FI indicating non-statistical variation and successful correction with p-values of 0.151, 0.157, and 0.088, respectively.

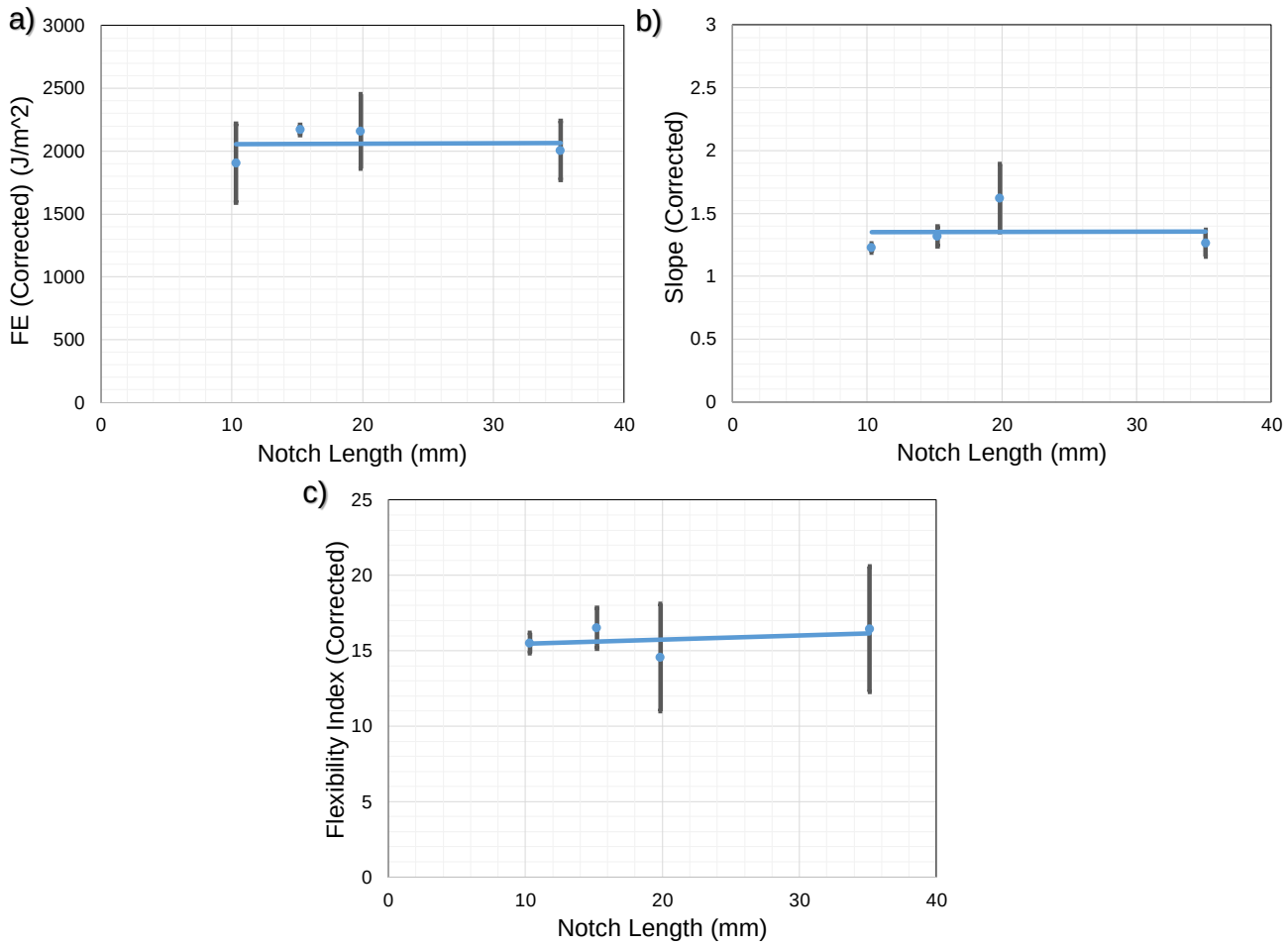

Figure 4.9: I-FIT results corrected for notch length: a) FE, b) slope and c) FI

4.4 Loading Rate Impact Evaluation

The loading rate impact was studied using 20 samples tested at 0.7, 6.25, 25, and 50 mm/min. Figure 4.10 shows the variation of the load vs displacement curves from representative specimens. As expected, the peak load, work of fracture, and post-peak slope increased at faster loading rates. Due to its viscoelastic behavior, AC becomes stiff and brittle at higher loading rates, thus resulting in an increase in the peak load and faster crack propagation (represented by the high post-peak

slope). In addition, as the loading rate increases, the material becomes less compliant in the pre-peak portion of the load vs displacement curve.

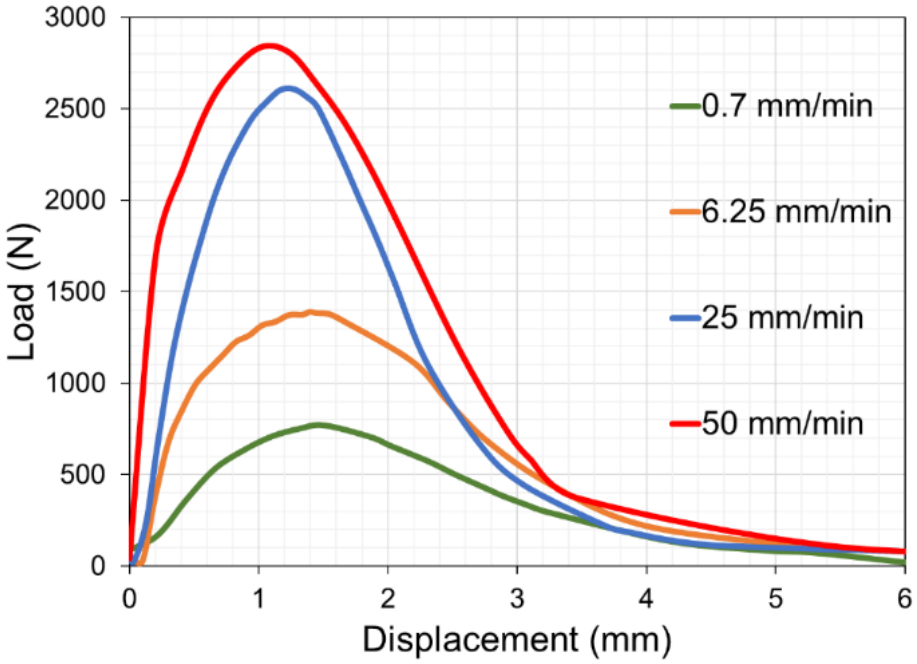

Figure 4.10: Load vs displacement curves for representative specimens at different loading rates

The I-FIT results for the loading rate variation are shown in Figure 4.11. As the rate increased, the FE, strength, and post-peak slope increased. The substantial increment of the slope resulted in a lower FI, indicating a stiffer response with higher loading rates.

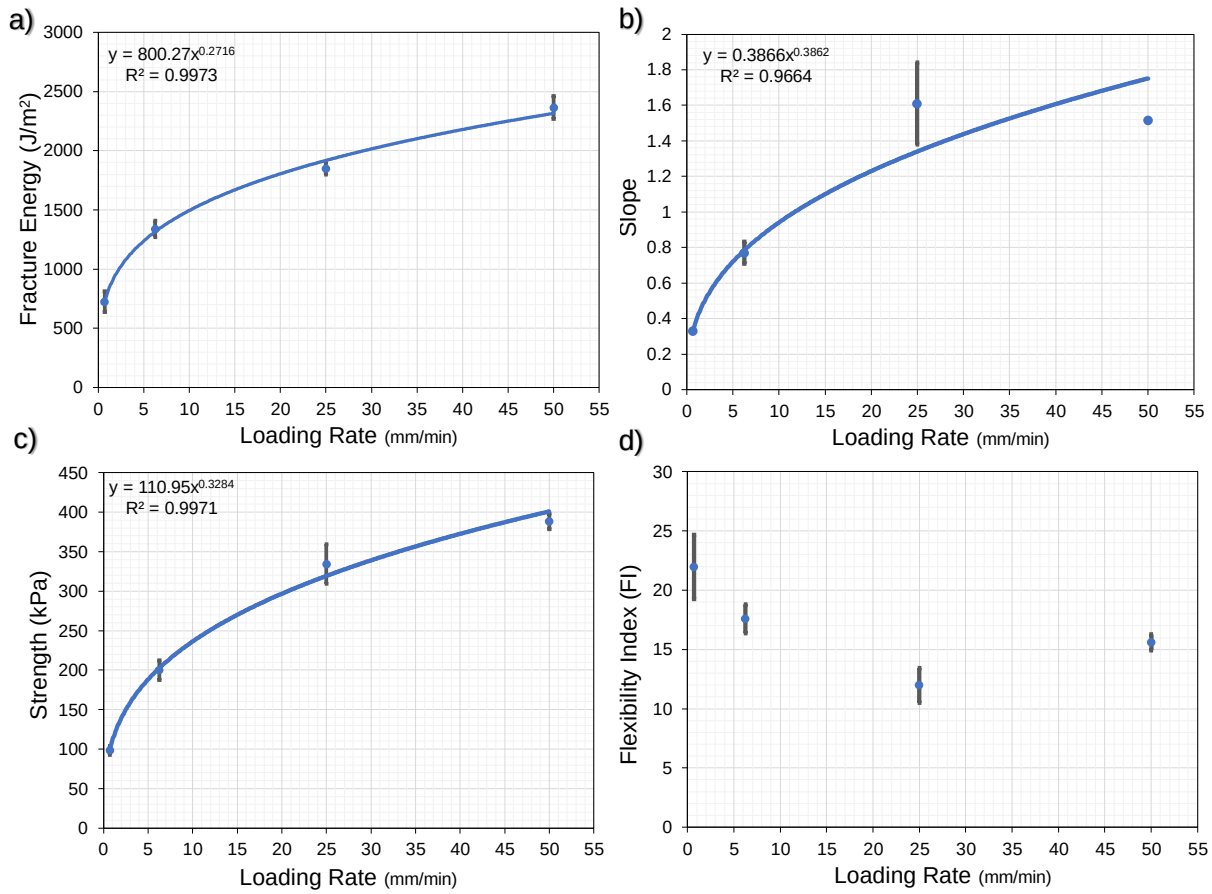

Figure 4.11: I-FIT results for the loading rate evaluation: a) FE, b) slope, c) strength and d) FI

A power regression fits the variation of the FE, strength, and post-peak slope with an R square of 0.99, 0.98, and 0.96, respectively, as shown in Figure 4.11. The power fit was used to shift all the results to the standard rate of 50 mm/min using the following equations:

Correction for Fracture Energy (G_f):

$$G_{fNL_{corrected}} = G_f * \left(\frac{50}{LR}\right)^{F(G)} \tag{4.3}$$

Correction for Post Peak Slope (m):

$$m_{NL_{corrected}} = m * \left(\frac{50}{LR}\right)^{F(m)} \tag{4.4}$$

F(G) and *F(m)* are the power coefficients found in the regression fit for the FE and slope, respectively. For Mix 1, *F(G)* and *F(m)* resulted in 0.2716 and 0.3862. The corrected FE, slope,

and FI are shown in Figure 4.12. From the converted values of Mix 1, an average FE of 2350 J/m^2 with a COV of 11.8% and a post-peak slope 1.67 with a COV of 15.5% were computed. This resulted in an FI of 14.3 with a COV of 15.6%. The one-way ANOVA analysis resulted in p-values of 0.015, 0.001, and 0.008 for the FE, strength, and FI, respectively. Although the correction performed in this analysis yield to a uniform FI, AC mixtures are highly susceptible to the loading rate with varying degrees of sensitivity depending on the mixture characteristics. Therefore, it is recommended to avoid any modification to the standard loading rate (50 mm/min).

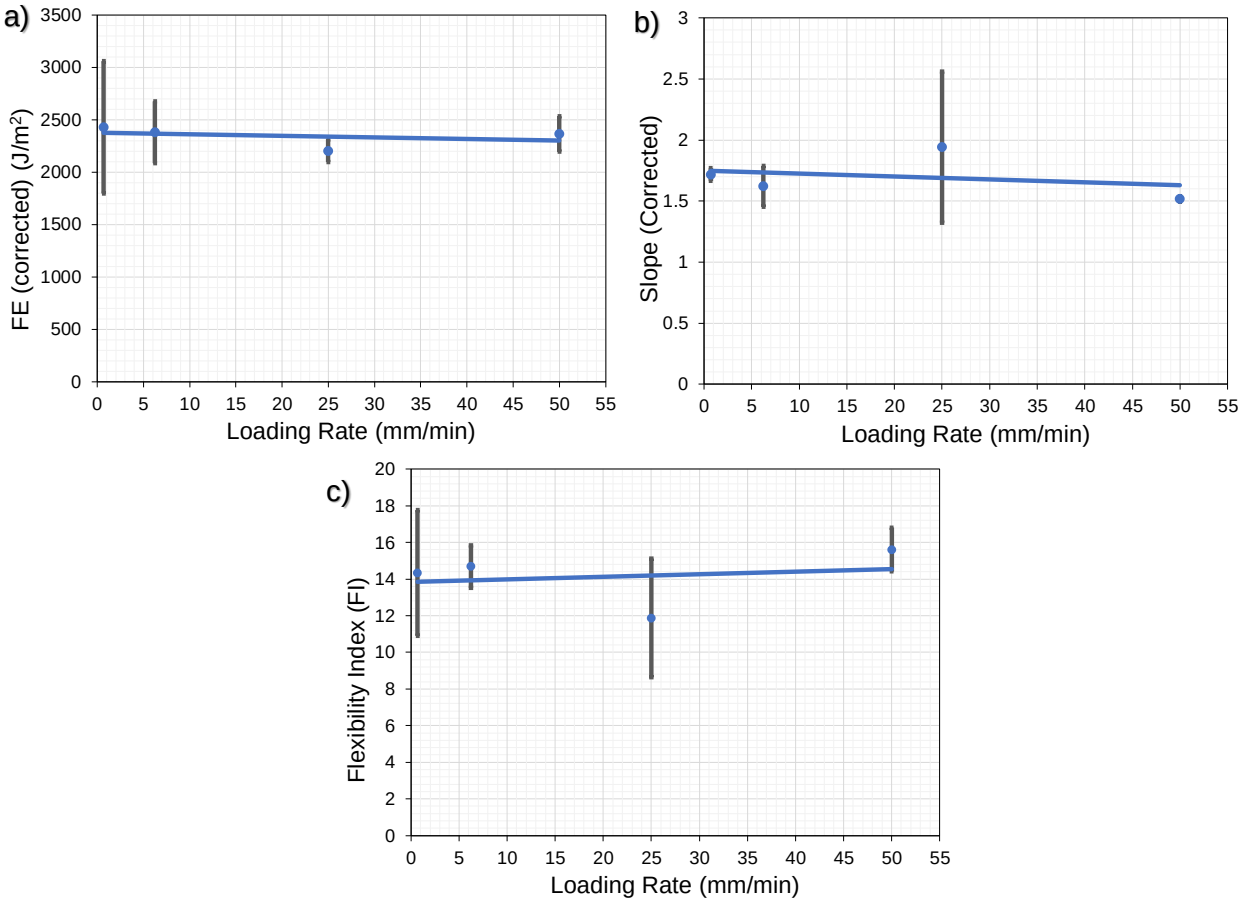

Figure 4.12: I-FIT results corrected for loading rate a) FE, b) slope and c) FI

4.5 Binder Evaluation

4.5.1 Binder Polymer Modification

Polymer modified asphalt are typically used in Illinois to increase the AC mix rutting, fatigue and low temperature cracking resistance. The addition of polymer typically increases the tolerance of the binder to deform and provides more flexibility. Therefore, it is expected to increase FI values of modified binders. In this section, two AC mixtures, with same aggregate gradation, were tested. Mix 1 uses a PG 64-22 and Mix 2 uses a PG 70-22 SBS polymer modified. Twelve specimens of Mixes 1 and 2 were prepared (6 per mix). Figure 4.13 shows a representative load vs displacement curve for the two AC mixtures. The polymer modified binders resulted in a higher peak load, work of fracture and post peak slope.

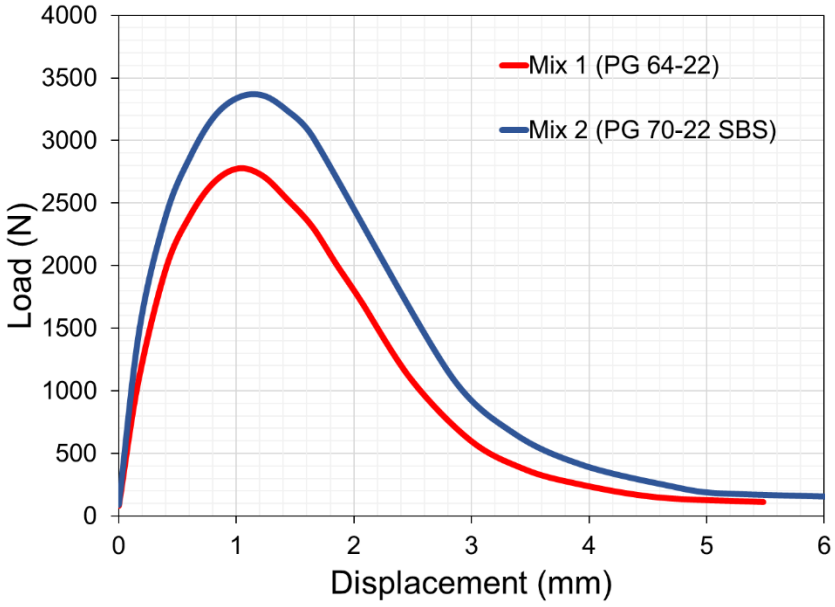

Figure 4.13: Load vs displacement curves for representatives specimens of AC mixes 1 and 2

Figure 4.14 shows the I-FIT analysis results for the AC Mixes. The polymer modified binders yields to higher FE and strength. However, the effect on the slope is not significant. Hence, the FI

for polymer modified AC mixture resulted to be higher than conventional binder for the set of mixes tested in the study.

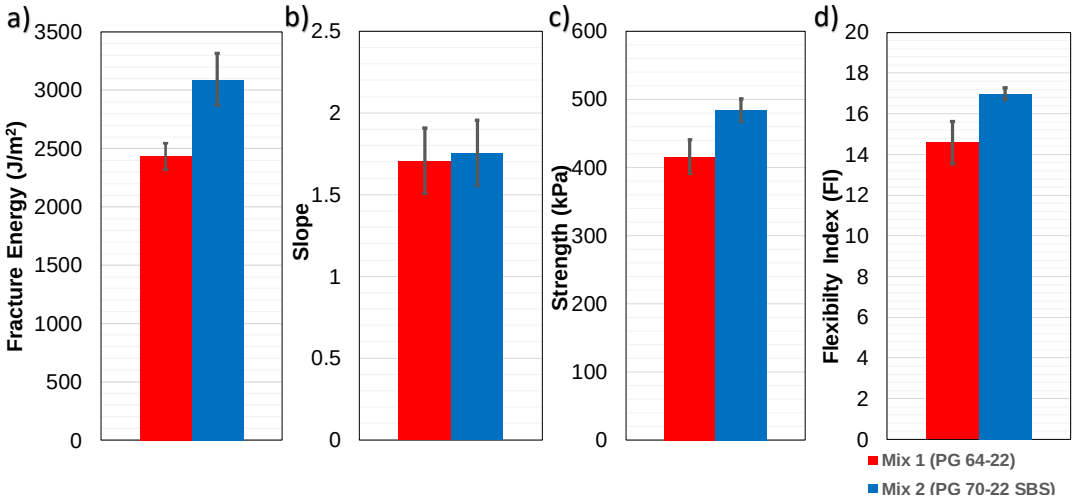

Figure 4.14: I-FIT results for the polymer modification evaluation: a) FE, b) strength, c) slope and d) FI

4.5.2 Storage Aging Impact

I-FIT specimens might be stored for extended periods of time before they are tested. Exposure to the environment may cause "storage aging" that could affect AC FI results. This section evaluates the impact of 60-day storage aging on I-FIT specimens of Mixes 1 and 2. A total of 24 specimens were fabricated under the same conditions; 12 specimens were tested within a week from sawing (Results were previously shown in Figure 4.13 and Figure 4.14) and the remaining specimens were kept in storage at 21^{o}C for 60 days after sawing before being tested. Figure 4.15 shows the load vs displacement curve from a representative specimen of the two AC mixtures at 0 and 60 days of storage. The storage aging caused stiffening of both AC mixtures. The aged samples reflected a higher peak load and post-peak slope. From the figure, it is difficult to observe any substantial change in the work of fracture.

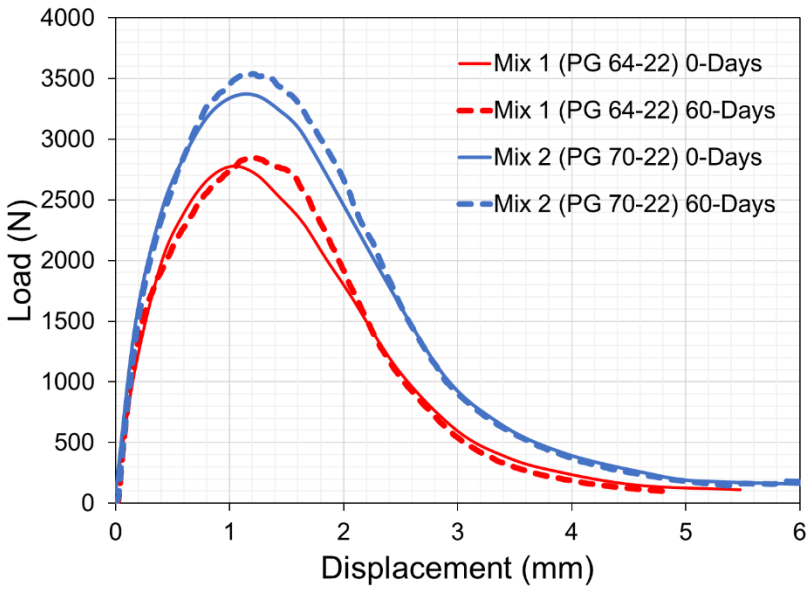

Figure 4.15: Load vs displacement curves for representatives specimens of AC mix 1 and 2 at 0 and 60 days aging

Figure 4.16 shows the I-FIT results for the storage aging evaluation. A decrease in FE and an increase in the post-peak slope were observed after 60 days of storage, but there was no significant variation in the strength. The reduction in the FE affected the FI results. The difference in FI resulted in p-values of 0.050 and 0.051 for AC Mix 1 and 2, respectively, that indicates a weak statistical difference. Therefore, storing I-FIT specimens for extended periods on the shelf can lead to a reduction in the FI.

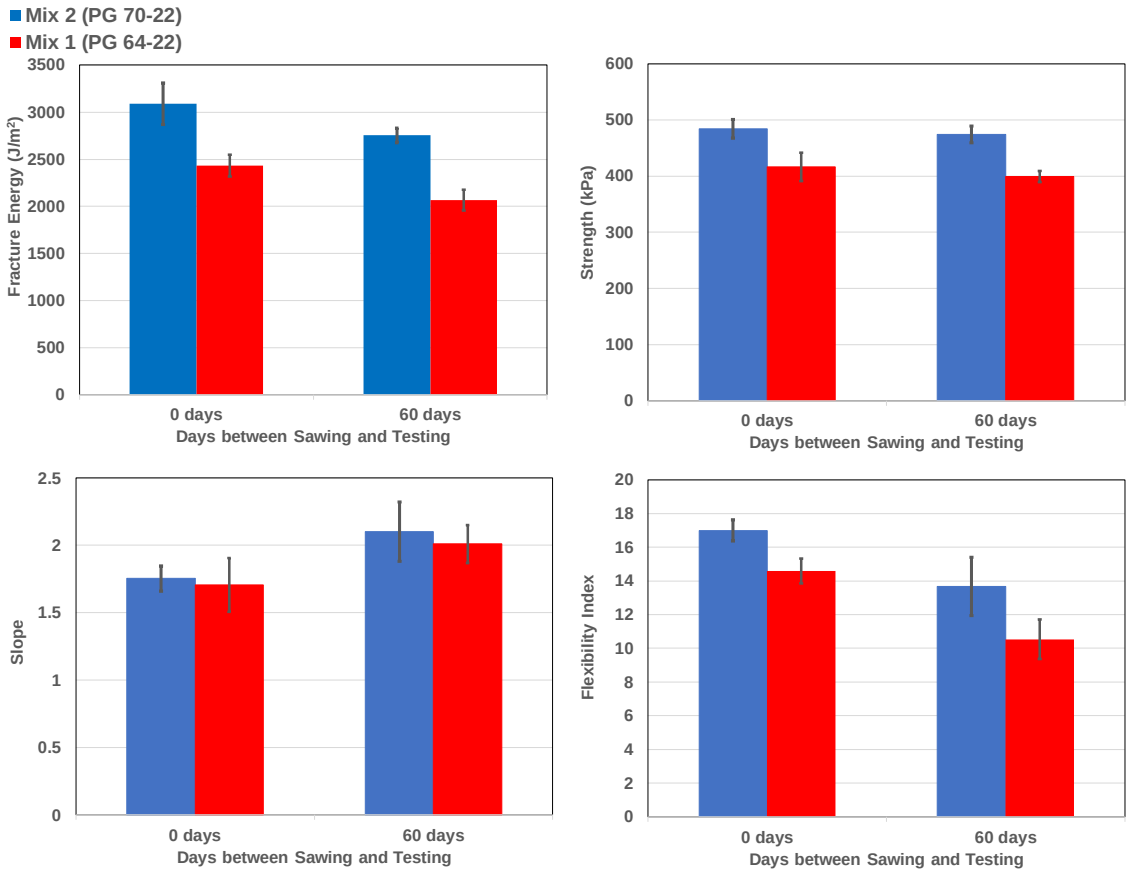

Figure 4.16: I-FIT results for the binder aging evaluation: a) FE, b) strength, c) slope and d) FI

4.6 Summary

In this chapter the effect of I-FIT specimen's thickness, air void content, notch length, loading rate, and polymer modification were investigated. It was observed:

- Thickness: as the thickness increased, post-peak slope increases; hence, FI decreased and the correction factor from Al-Qadi et al, 2015 was found to be acceptable.
- Air Voids: AC air void content may not significantly affect FE or specimen's strength. However, post-peak slope may decrease, resulting in an increase in the FI. The correction factor from Barry et al, 2016 was found to be acceptable.

- Notch Length: An increment of the notch length resulted in a decrease in the FE, strength, and post-peak slope. A correction factor is proposed in this study to account for the variation.
- Loading Rate: at faster loading rates, the AC mix experience a stiffer behavior resulting in an increase of the FE, post-peak slope, and strength.
- Binder Effect: the use of a polymer-modified binder resulted in higher FE and FI.

CHAPTER 5 : FRACTURE PROCESS ZONE

5.1 Fracture Process Zone Development

To understand the relation between the AC microstructure and I-FIT, the geometric properties of the fracture pressure zone (FPZ) were studied. As mentioned in Section 3.2, this study used digital image correlation (DIC) to measure the opening strain field (e_{yy}). Strains larger than 3000 με were defined as the FPZ based on the threshold approach identified by Doll et al (2017), and Hill and Buttlar (2016). Due to the use of Vic2D, this study is limited to analyzing deformed images before a macro crack develops. Typically, a macro crack starts to develop following the peak load. Therefore, the study focuses on evaluating FPZ development up to the peak load. Using the I-FIT standard loading rate of 50 mm/sec; it takes from 1.5 to 2 sec to reach the peak load. A camera frame rate of four frames per sec (fps) allows capturing five to six images in this region. Figure 5.1 shows FPZ development before the peak load for an AC Mix 1 sample tested according to standard I-FIT requirements. The load vs displacement curve of Figure 5.1 shows the instant when each image was taken with respect to the load vs displacement curve. Then, the FPZ mapping for Images 21 to 26 is shown. The red area is the zone where the strains exceed the threshold, and the blue area is the zone where strains are below the threshold. The FPZ started to occur in Image 23 at 83 % of the peak load. It was observed that the FPZ started to develop when the load reached approximately 70 to 85 % of the peak load. As a result, trying to compare the strain fields forming at the same absolute load level was not feasible. In addition, it could be challenging to find pictures corresponding to the same load for the different experiments at the frame rate used. Therefore, the FPZ area at the peak load was used to compare the damage between specimens.

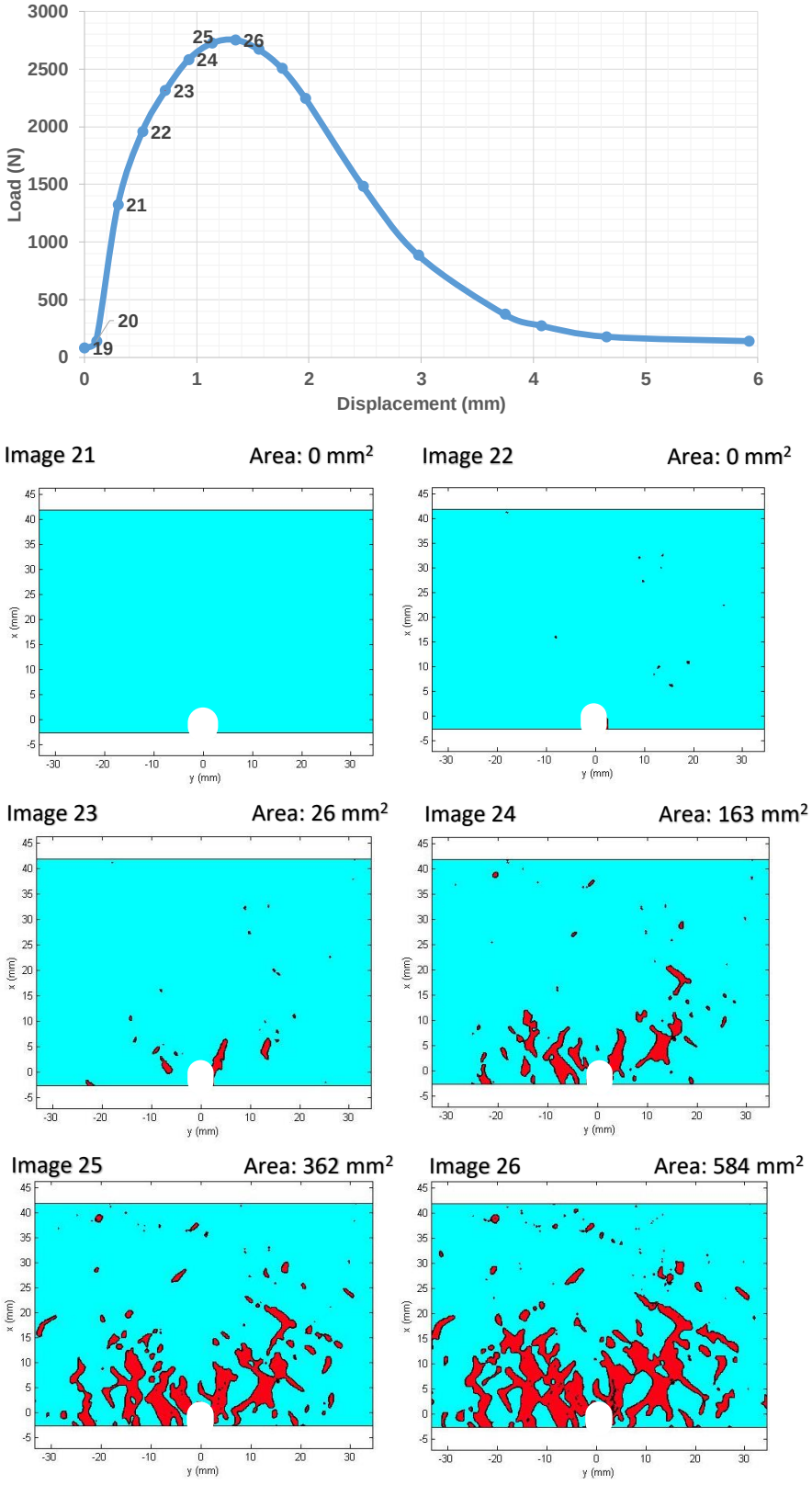

Figure 5.1: Fracture process zone development before the peak load for AC mix 1 tested at I-FIT standard conditions

5.2 Strain Field Characteristics

Figure 5.2 shows the opening strain profile per pixel for a typical 50 mm thickness I-FIT specimen of AC Mix 1 at the peak load obtained following image correlation. The vertical axis is the opening strain magnitude measured while the horizontal axis corresponds to the geometric location (X and Y) where the strain occurred. The origin was set to be located at the notch tip. Figure 5.2-b shows the opening strain profile relation to the surface of the I-FIT specimen; the strain concentration effect due to the existence of a flaw (the notch) could be noticed. The largest strains were concentrated in the region close to the notch tip. The strain decreased as the distance from the notch tip increased, but not in a continuous or gradual manner due to heterogeneity of the material.

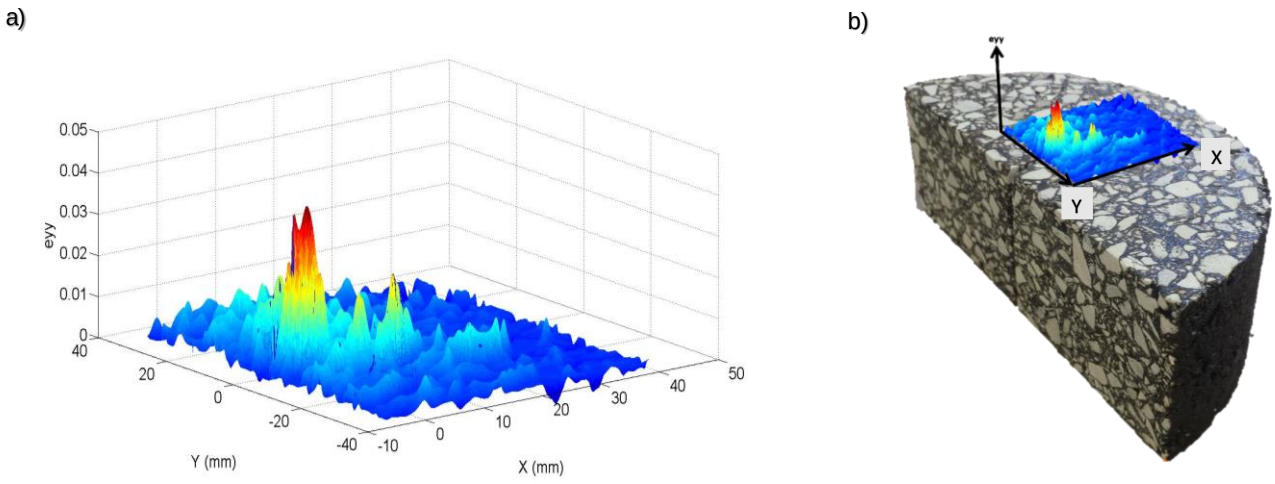

Figure 5.2: Opening strain profile (e_{yy}) for a AC mix-1 I-FIT specimen b) relative location of the opening strain profile in the surface of an I-FIT specimen

The effect of the aggregate structure to the FPZ was reported by Doll, 2014. In this study, a similar approach was used to verify that the FPZ shape is caused by the aggregate structure. Before the application of the speckle pattern, a picture of the unpainted specimen was captured to superimpose the strain field (at the reference frame) over it. Superimposition of the strain field was done

manually by selecting control points seen in the unpainted and experimental pictures. Typically, air voids were used as the control points. By changing the transparency of the strain field, it was possible to have the strain field and aggregate structure on the same image at the micro scale as shown in Figure 5.3. To check accuracy of the superposition, the process was repeated three times on different days for the case shown in Figure 5.3, then the final shrink size and location of a reference points were compared as shown in Table 5.1. The shape of the FPZ is caused by the heterogeneous nature of AC. Most of the deformation occurred around the aggregates (in the AC matrix) since aggregates are stiffer and the binder is more compliant. The tests conducted for AC Mix 1 and Mix 2 in the following sections of this study indicate a trend consistent with the findings by Doll et al. (2017).

Table 5.1: Accuracy of the superimposition

Original Image Size	6225	4150				
	Final Size		Location of the Reference Point		Location of the Reference Point	
Positioning:	X (pixel)	Y (pixel)	X (pixel)	Y (pixel)	X (mm)	Y (mm)
1	3541	2350	1570	1270	15.099	12.214
2	3638	2423	1632	1331	15.695	12.801
3	3690	2450	1648	1346	15.849	12.945
Difference	149	100	78	76	0.750	0.730
%Error	2.40	2.41	1.25	1.83		

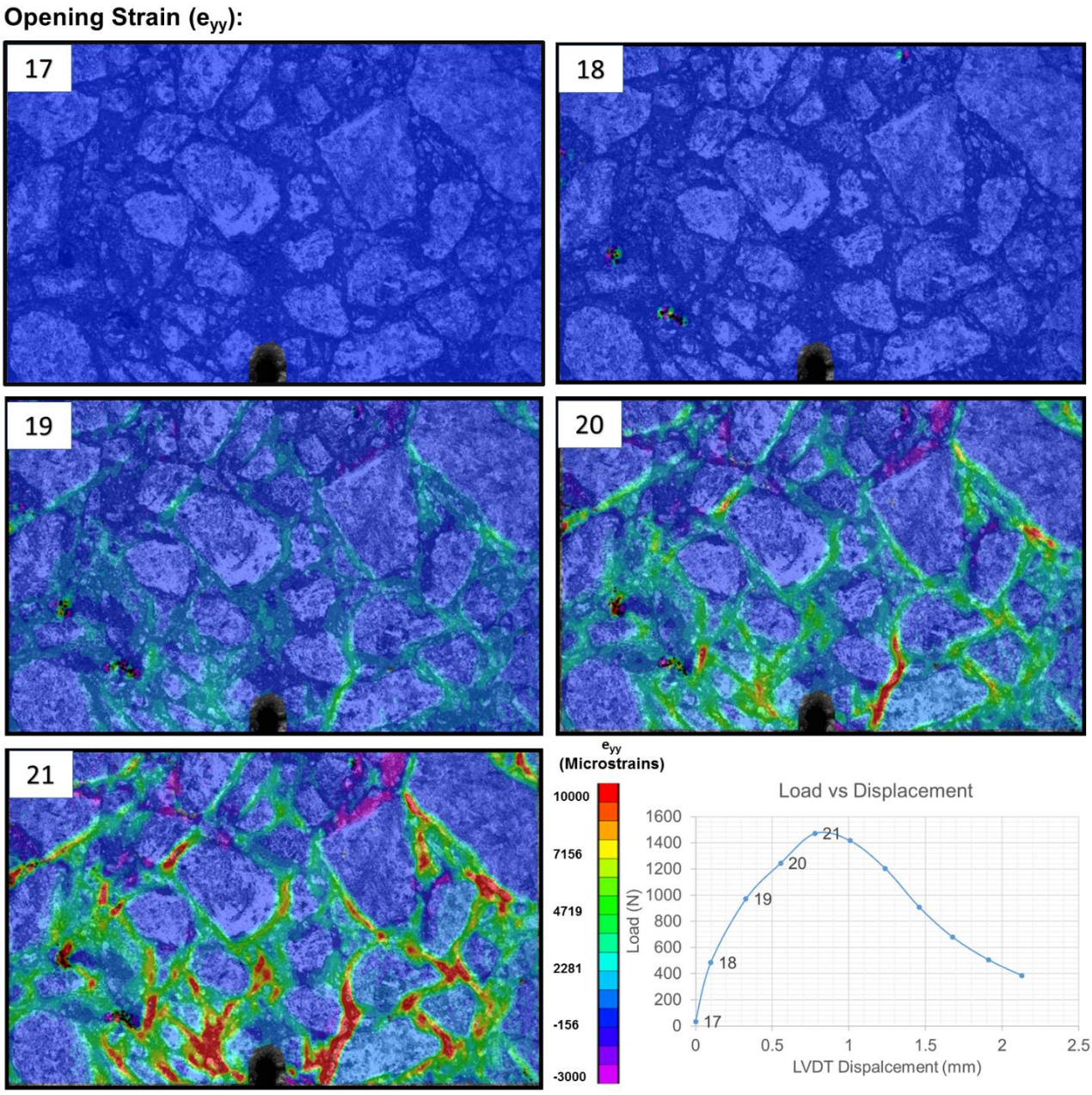

Figure 5.3: Superimposition of the strain field over the aggregate structure for an I-FIT specimen (Mix 1, 25°C, 50 mm/min)

5.3 Thickness Effect on the FPZ

DIC was conducted using the specimens presented in Section 4.1 to evaluate the impact of thickness on the FPZ. The average area is reported in Figure 5.4 smaller thicknesses (25, 30 and 40 mm) have larger FPZ areas than those of thicker specimens (45, 50, 60 mm). Figure 5.5 shows the FPZ at the peak load for one representative specimen of each case. On the top-right corner of each image, the total I-FIT area covered by the FPZ is reported. The images show a decrease in the FPZ size as the thicknesses increases between 25 mm until 40 mm. Then for specimens higher than 45 mm, the FPZ size was kept relative constant. The small thickness specimens are more compliant as previously described in section 4.1. This suggests that the failure is driven by the deformation of the specimen due to excessive crack tip deformations. At increased thicknesses, deformations are reduced due to overall increase in structural capacity of the specimen and partly due to higher confining stresses resulting in smaller FPZ size. However, when thickness is approximately greater than 40 mm, FPZ converged to a constant value. This transition may be attributed to the fact that the rate of change in the deformations with increasing thickness reduced and stress fields reached a more critical level. This may have resulted in crack tip microstructural damage governed by stress fields with relatively small or insignificant rate of change when thickness changed from 45 to 60 mm change.

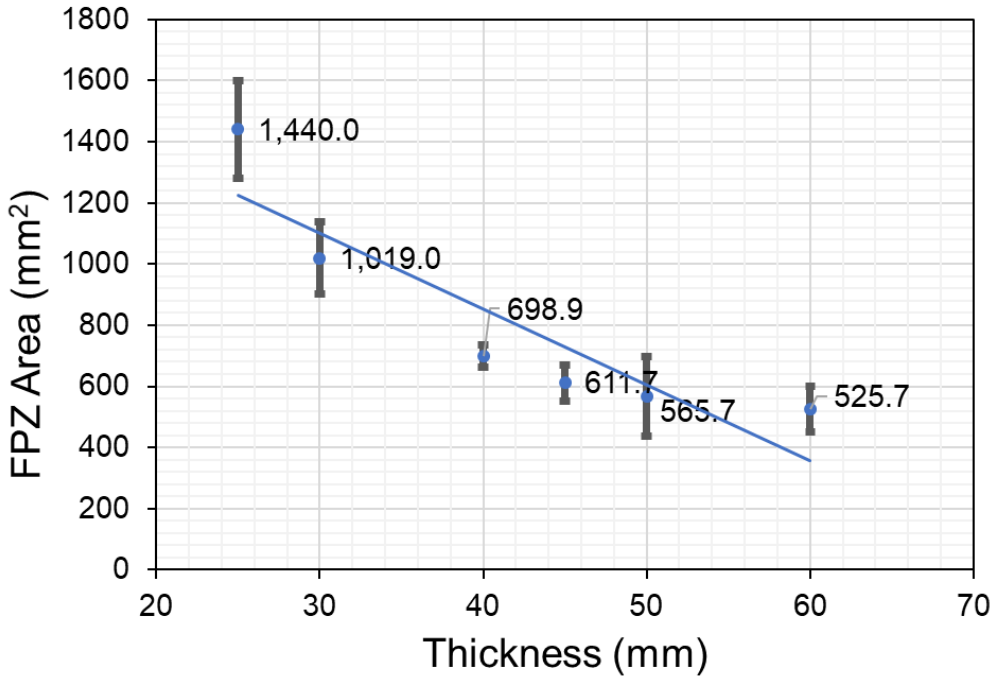

Figure 5.4: Average FPZ area for the tested thicknesses

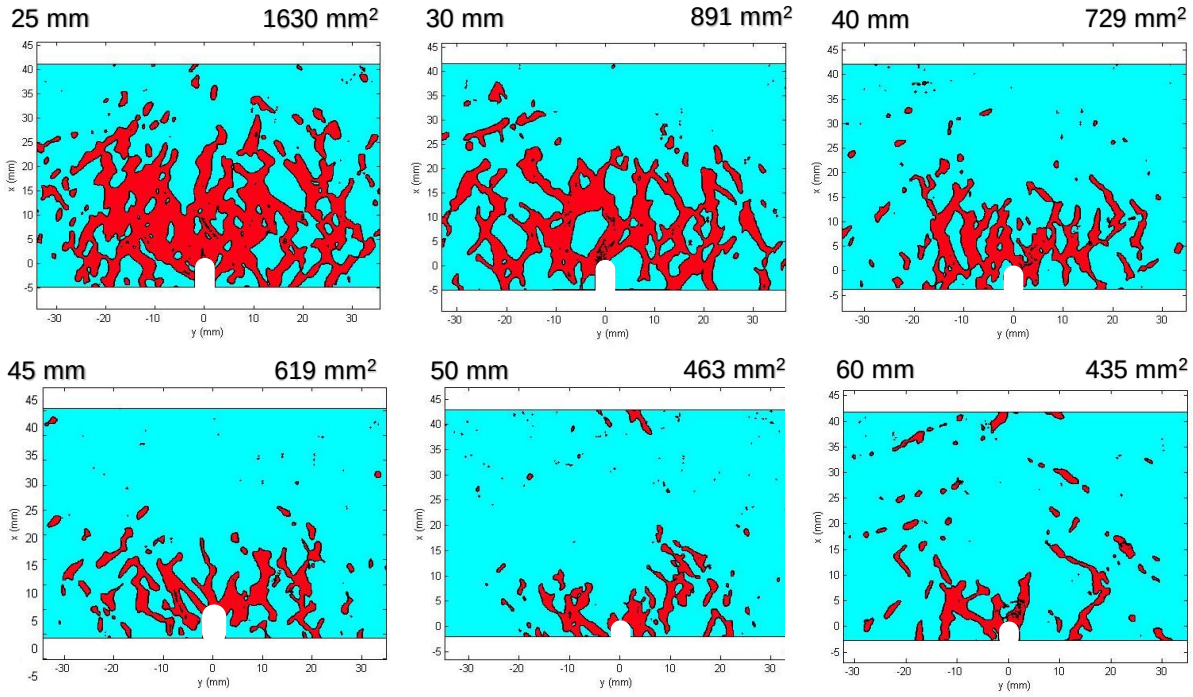

Figure 5.5: Fracture Process Zone for representative I-FIT specimens at the peak load for different specimen thicknesses

The size of the FPZ from its initiation up to the peak load is plotted for the same representative specimens of Figure 5.6a; the same trend shown in Figure 5.5 is noted. The FPZ decreased with the larger thickness. In comparison with the load vs displacement curve, it was observed that the FPZ area decreased with the increase in the work of fracture and peak load.

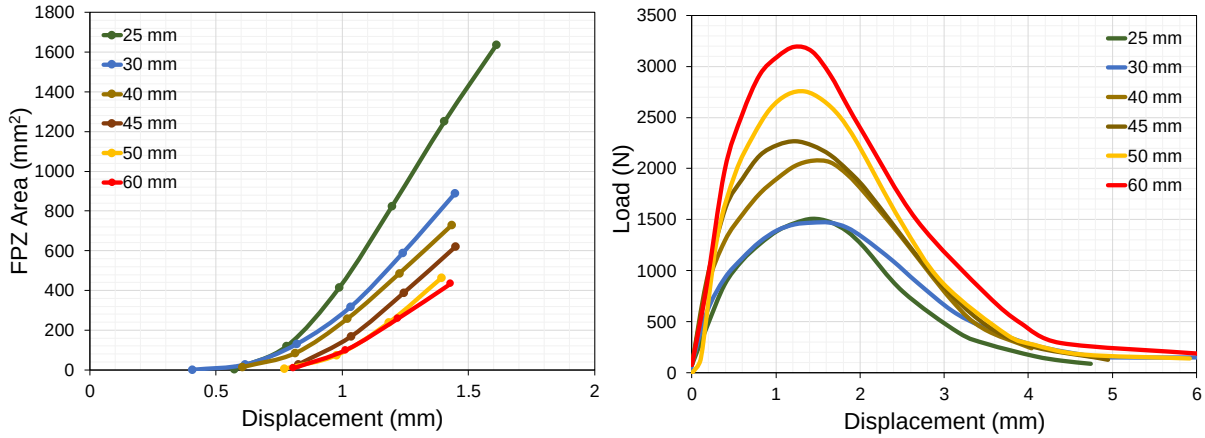

Figure 5.6: a) FPZ area vs displacement before the peak load, b) load vs displacement curves

Doll et al. (2017) suggested that extended FPZ area may record larger opening strains magnitudes than smaller FPZ areas. This can suggest that, as the FPZ area increases, larger opening strains occupies a larger fraction of the FPZ area than smaller opening strains. To evaluate this claim, considering the full strain distribution (instead of measuring only the peak values), two histograms were prepared using the results of the representative specimens as shown in Figure 5.7 and Figure 5.8. In both figures, the horizontal axis corresponds to the opening strain from 3000 με up to 13100 με divided into equal size bins of 100 με. The vertical axis of Figure 5.7 and Figure 5.8 shows the absolute area measured for each strain range and the percentage that each strain bin occupies within the FPZ respectively. In the thickness evaluation, the FPZ area increases as the thickness decrease therefore if the claim is true, it was expected to see that as the thickness decrease, the area that the large strain bins (> 8500 με) occupy increases while the area that the smaller strain bins (< 8500

με) occupy decreases. However, this trend was not evident as seen in Figure 5.7. The figure shows that both the large sand smaller strain bins increased as the thickness decrease. Therefore, the increase in FPZ area was reflected uniformly in all the strain bins ranges.

In Figure 5.8 a second evaluation was done by computing the percentage that each strain bin occupies within the FPZ. If the claim is true, the histograms will reflect that large strain bins (> 8500 με) would occupy larger percentage of the FPZ area. The figure shows that the internal FPZ strain distribution was similar between the six cases and no significant trend was found. As a result, the change of the FPZ area affect uniformly all the strain ranges and no redistribution of the strain was observed.

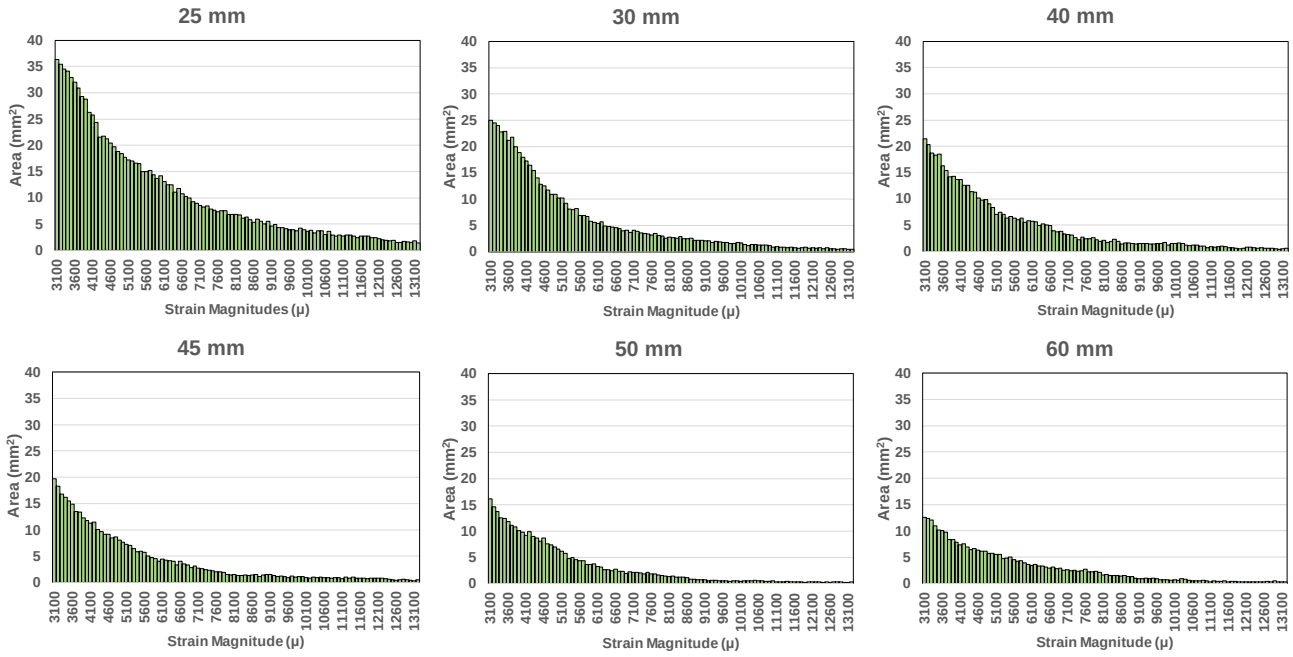

Figure 5.7: Total area distribution for opening strain ranges of representative I-FIT specimens of 25, 30, 40, 45, 55, and 60 mm thicknesses

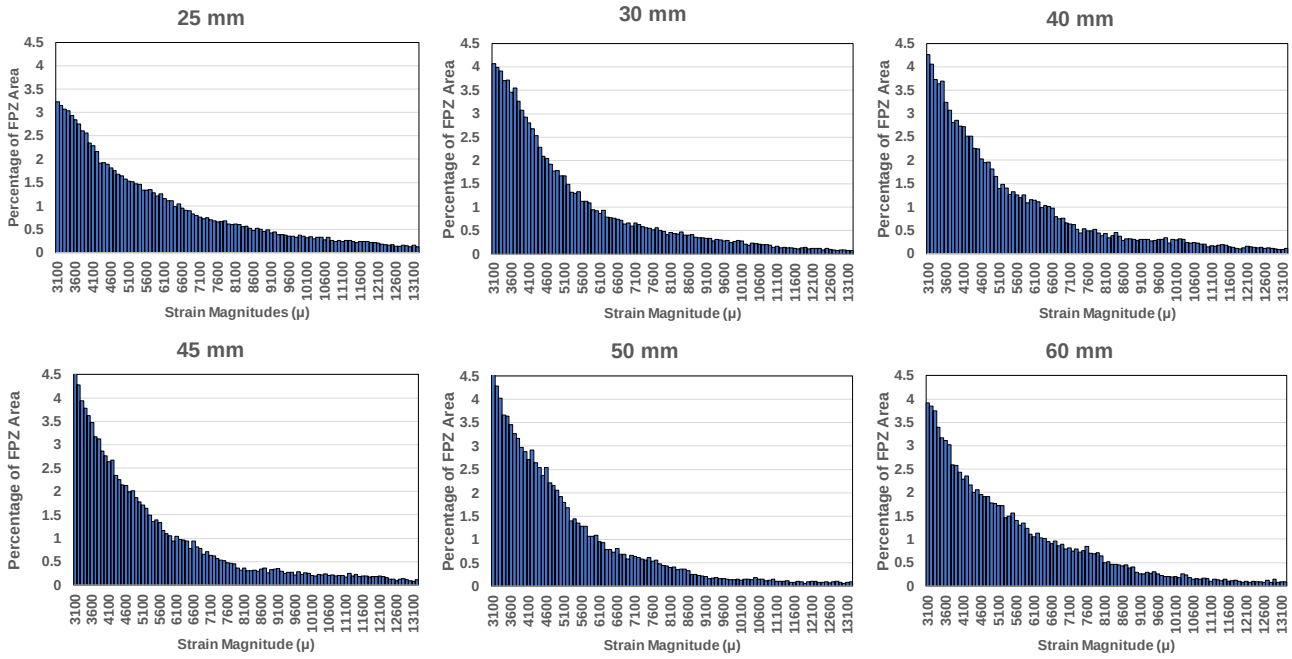

Figure 5.8: Percentage of fracture process zone area distribution for opening strain ranges of representative I-FIT specimens of 25, 30, 40, 45, 55, and 60 mm thicknesses

5.4 Specimen Air Void Content Effect

The impact of the air voids in total mix (VTM) on the FPZ size was analyzed using the DIC measured strain field of the samples tested in Section 4.2. The samples with 2 and 4% air voids failed before at least two images were captured due to the above-mentioned increased stiffness. Only the results at 6, 8, and 10 % are reported in

Figure 5.9. The average FPZ area increased with larger air voids content. Figure 5.10 shows the FPZ at the peak load for one representative specimens where the reduction in the FPZ can be noticed.

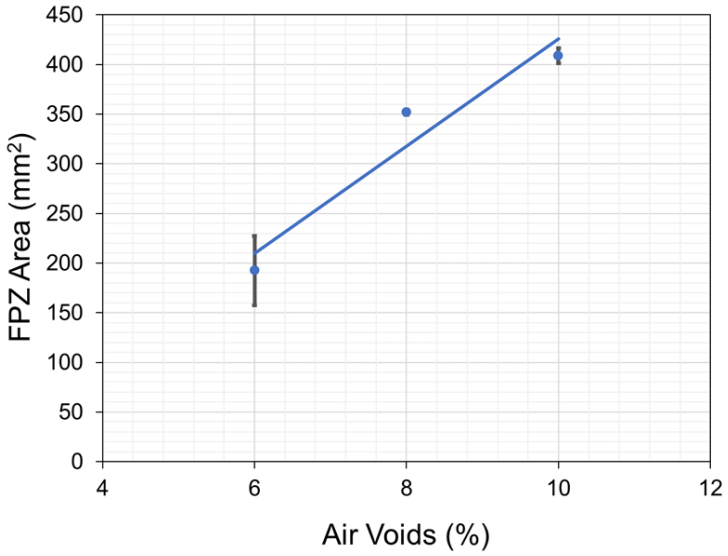

Figure 5.9: Average fracture process zone area for 6, 8, and 10% VTM

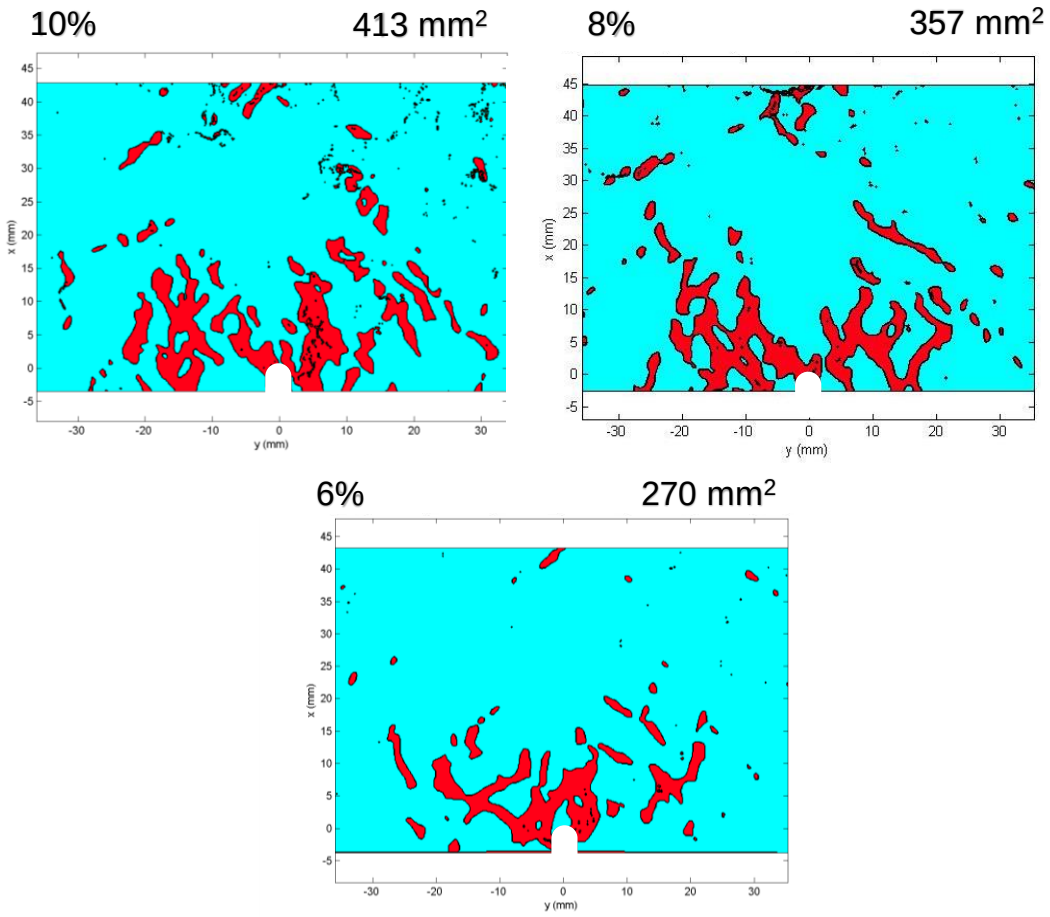

Figure 5.10: Fracture process zone at the peak load for representative I-FIT specimen at 10, 8, and 6% VTM

Figure 5.11 shows the size of the FPZ from its initiation up to the peak load for the same representative specimens of Figure 5.10. The size of the FPZ increased with respect to the air void content regardless of the displacement level where the measurement was taken. In addition, the same trend illustrated in Figure 5.5 can be observed at the peak load. Similar to the effect of thickness on I-FIT specimens, the decrease in the FPZ area coincides with the increase in the work of fracture and peak load. The air voids induced damage at the micro scale. Thus, when the air voids content, above a specific level, increased, micro cracks expanded into a larger area (FPZ area), thus reflecting the extend of the damage with increasing air voids. Consequently, the work of fracture and the peak load were reduced.

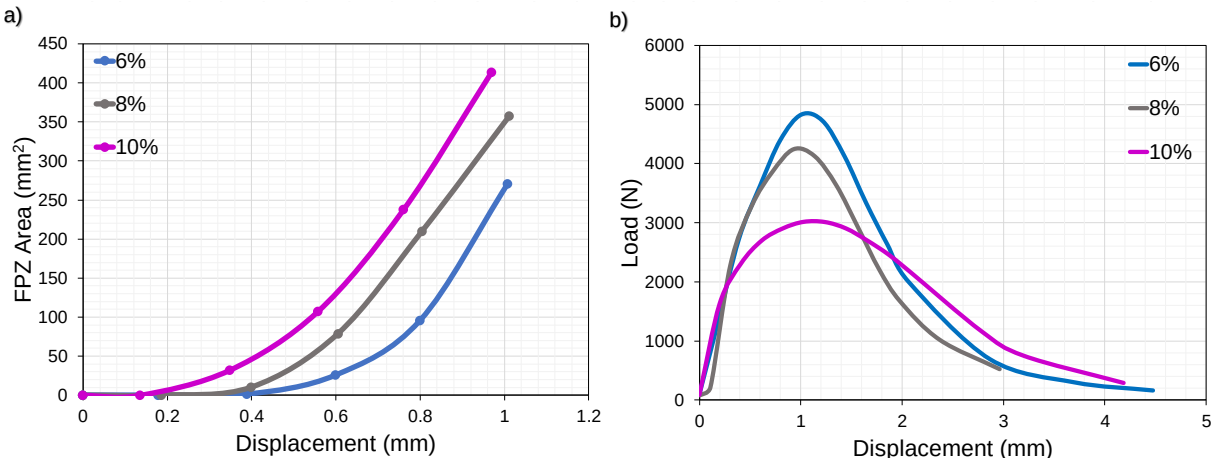

Figure 5.11: a) Fracture process zone area vs displacement before the peak load b) load vs displacement curves for air voids evaluation

5.5 Effect of Notch Length

The FPZ was studied for different initial notch lengths using DIC for the specimens presented in Section 4.3. Average FPZ zones are reported along with the standard deviation (error bars) in Figure 5.12. The FPZ at the peak load for one representative specimen of each case is shown in

Figure 5.13. It can be noticed that the average FPZ area decreased with the longer notches, which agrees with Li and M. Marasteanu (2010).

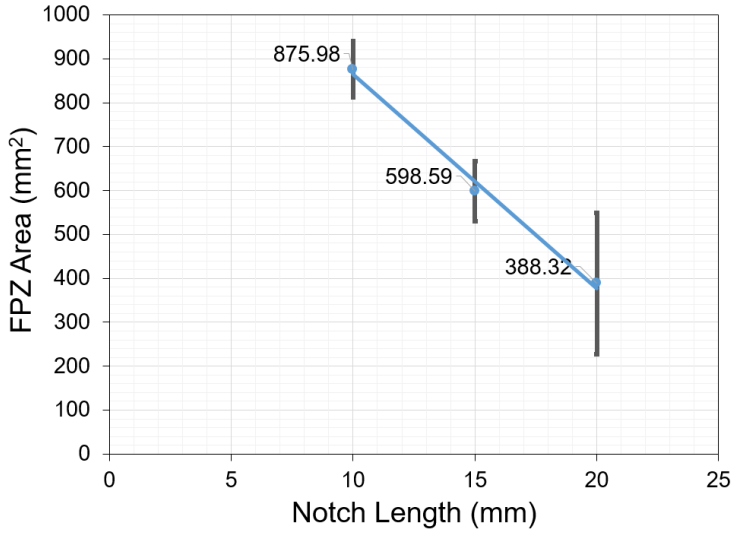

Figure 5.12: Average fracture process zone area and standard deviation (error bars) for 10, 15, 20 and 35 mm notch length

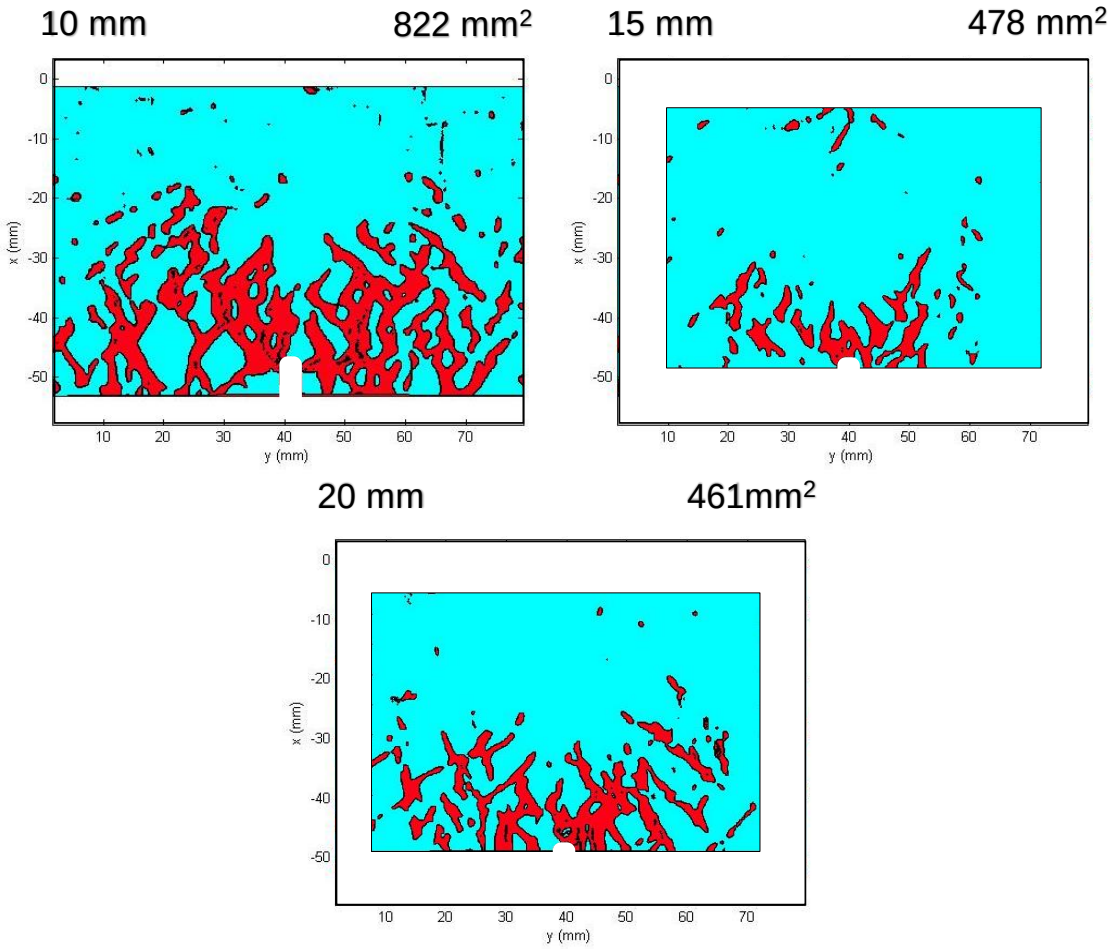

Figure 5.13: Fracture process zone at the peak load for 10, 15, 20, and 35 mm notch length

Figure 5.11 shows the size of the FPZ from initiation to the peak load and the respective load vs displacement curves for the representative specimens of Figure 5.13. The decrease in the FPZ area did not coincide with the increase in the work of fracture and peak load as was the case for the change in thickness and air voids.

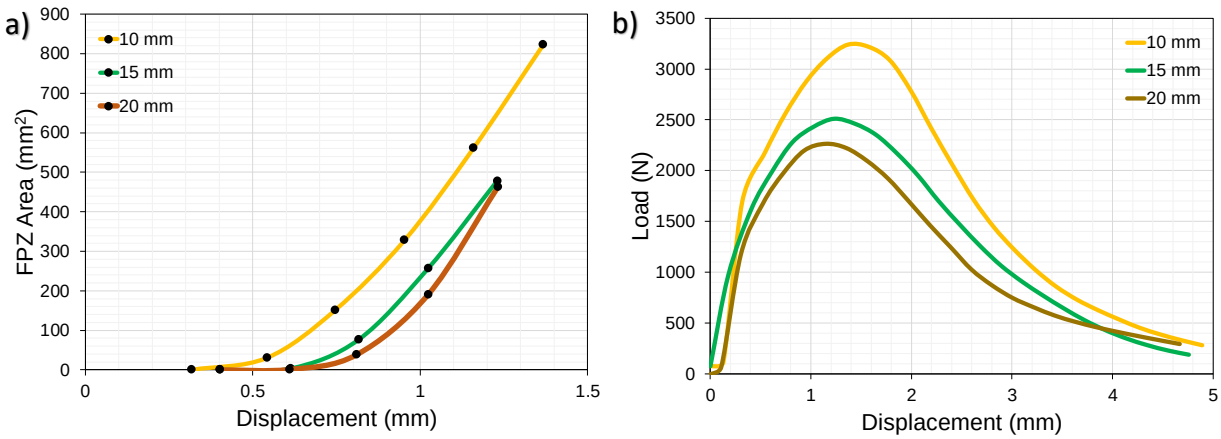

Figure 5.14: a) Fracture process zone area vs displacement before the peak load; b) load vs displacement curves for the notch length evaluation (for representative specimens)

Typically, larger FPZ correlates with specimens of lower peak load and FE; however, for long notch I-FIT this was not the case. Typical I-FIT specimens with 15 mm notch fails due to mode I fracture, the opening strain (considered in the FPZ) is the main energy dissipation mechanism at failure as shown in Figure 5.15-a. Compressive strains concentrate close to the loading point and does not have a major influence on failure. However, when the notch length is long, the energy is dissipated by both, compression and tensile strains acting close to the notch tip as shown Figure 5.15-b. Since our FPZ definition considers only opening tensile strains, there is an impression that there is less deformation (smaller FPZ) at these specimens. Figure 5.16 shows the DIC results where the strain field for specimen with short notches (10, 15 mm) is mostly dominated by the opening tensile strain (red colors). For longer notch length, both the compressive (blue colors) and tensile strains dominate the deformation occurring close to the crack tip and the area occupied by the tensile strains (FPZ area) is smaller. The Von-Mises strain fields shown in Figure 5.17 indicates that that the total deformation, considering only the strain components e_{xx}, e_{yy}, and e_{xy}, was practically similar between the four cases tested.

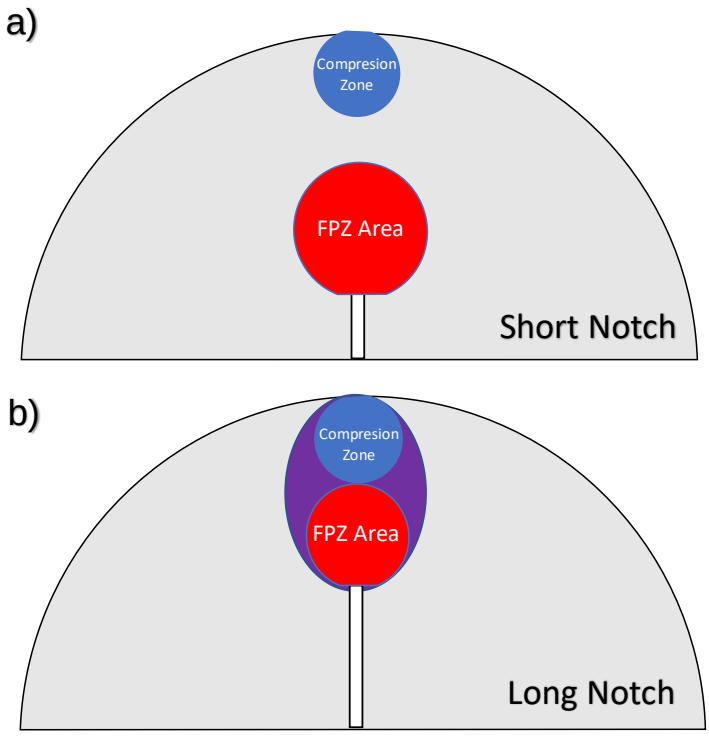

Figure 5.15: Diagram illustrating the two main deformation regions occurring in an I-FIT specimen, on red, the FPZ area (opening tensile strain) and blue the compression region due to the applied load

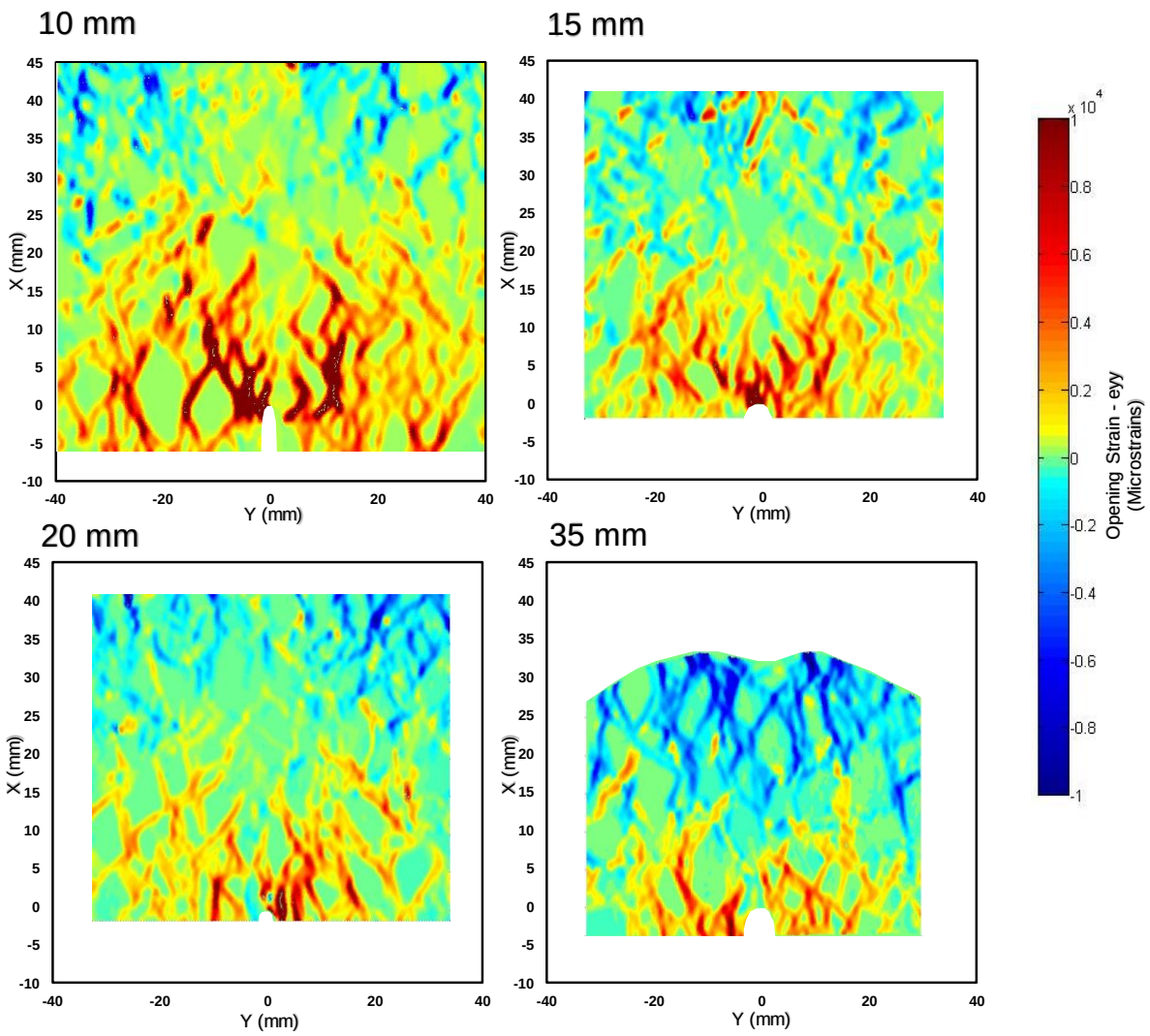

Figure 5.16: Strain fields (e_{yy}) at the crack tip for the representative specimens at the peak load

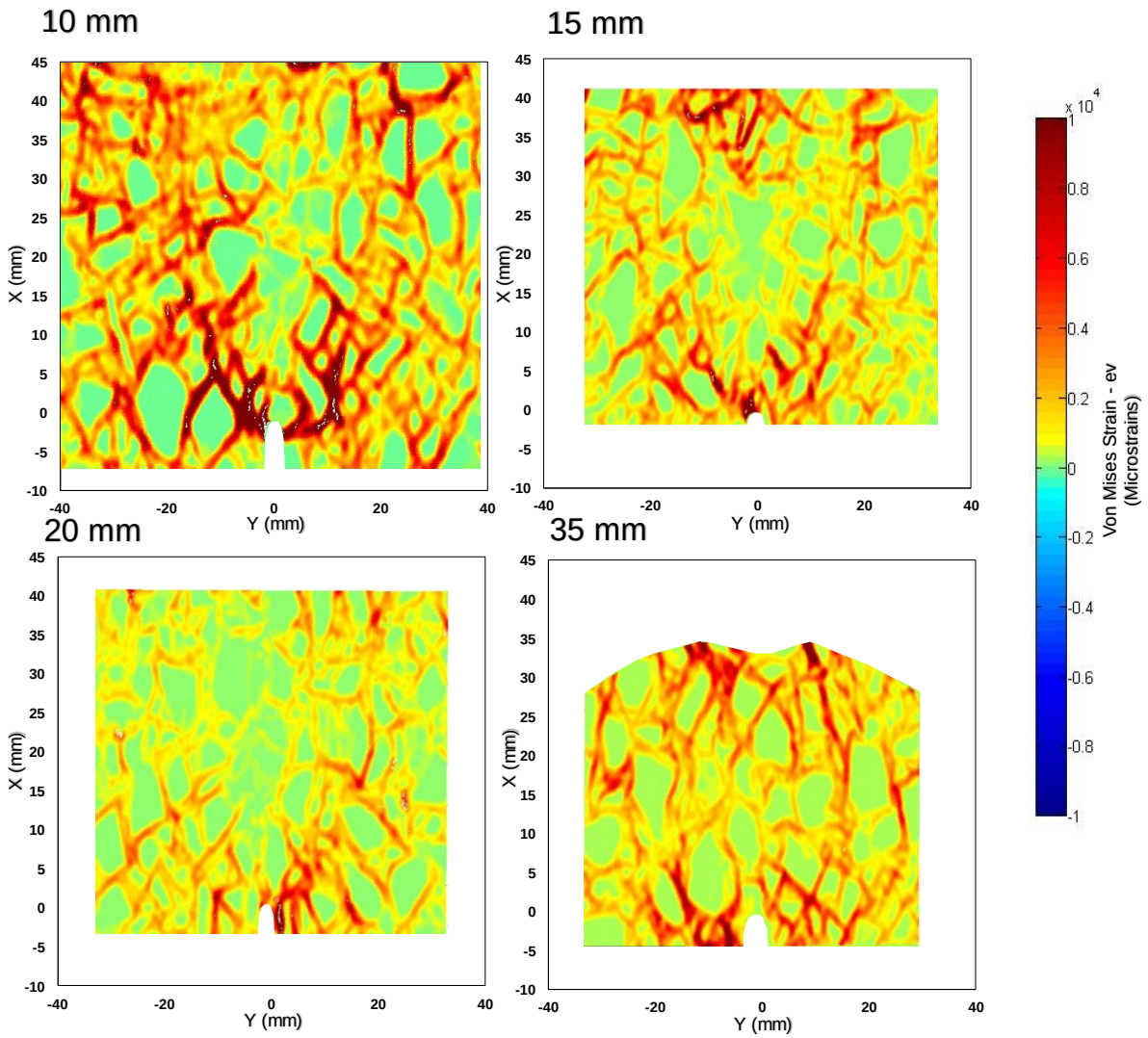

Figure 5.17: Von-Mises strain fields (e_v) at the crack tip for the representative specimens at the peak load

5.6 Effect of Loading Rate

Figure 5.18 shows the average FPZ area at the peak load obtained for the specimens (see Section 4.4) tested at 0.7, 6.25, 25, and 50 mm/min. The FPZ area was decreased at faster loading rates, Figure 5.19 AC becomes stiffer under faster loading rates. The viscoelastic matrix does not relax and deforms at faster loading rates, thus resulting in a smaller FPZ area. The size of the FPZ during the pre-peak portion of the curve is shown in Figure 5.20-a. As the loading rate increased, the area

decreased at the corresponding displacement levels before failure. Comparing Figure 5.20-a with b, it is observed that the decrease in the FPZ area resulted from the stiffer response (increase of the work of fracture and peak load).

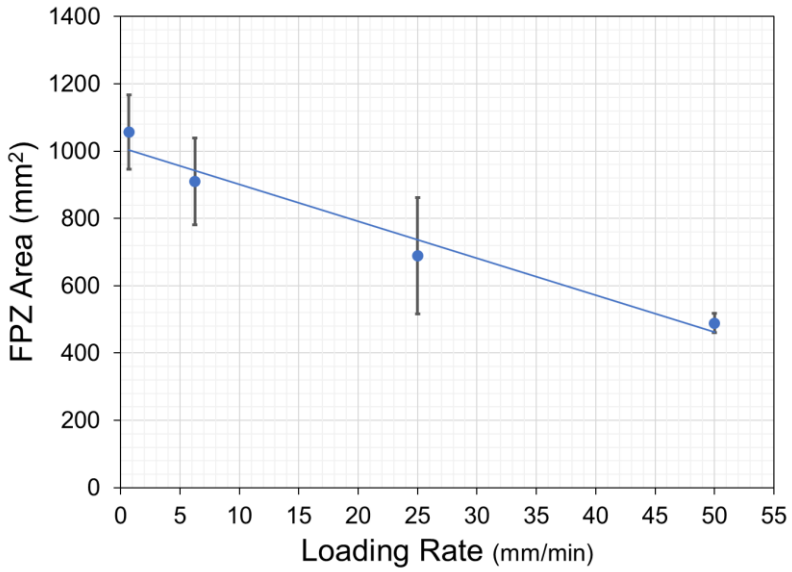

Figure 5.18: Average fracture process zone at the peak load for loading rates of 0.7, 6.25, 25, and 50 mm/min

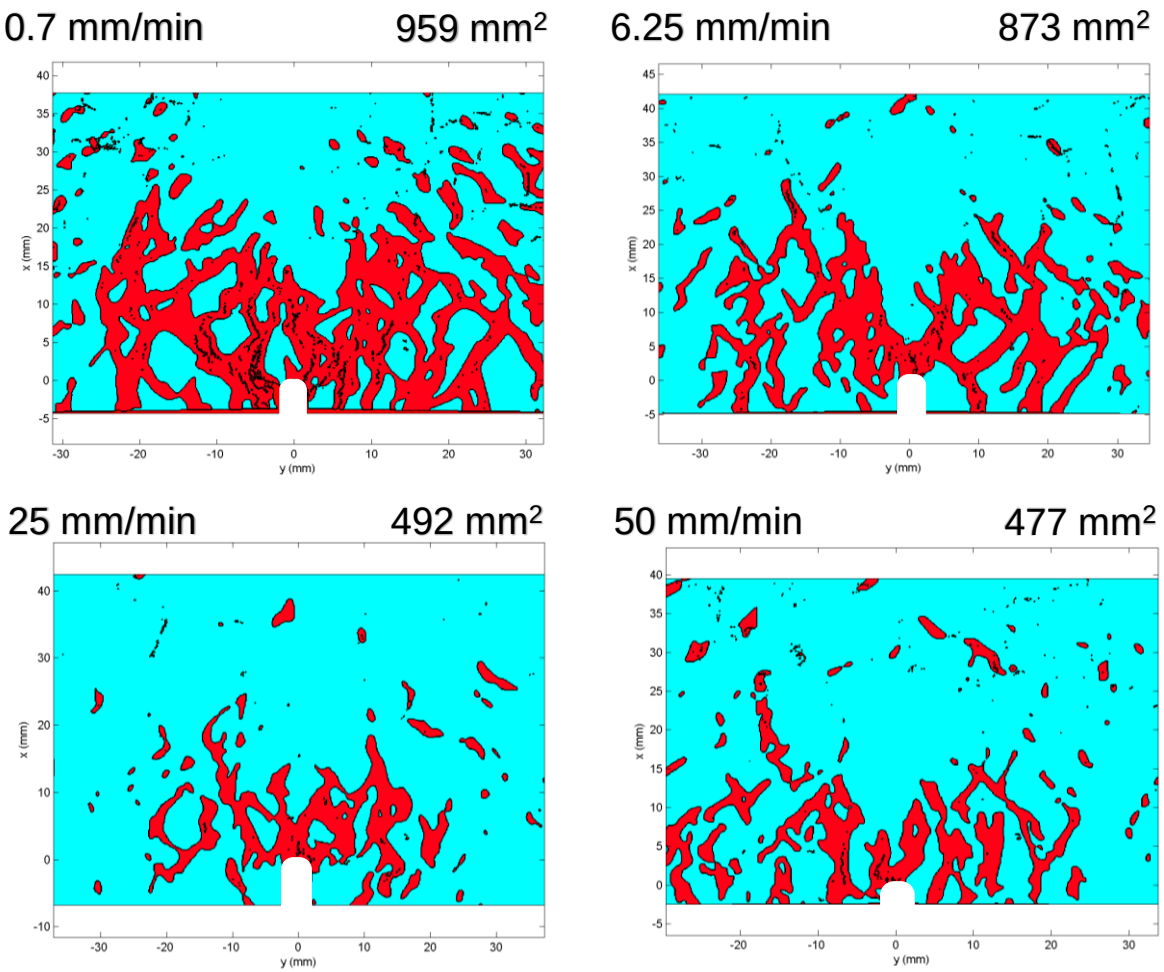

Figure 5.19: Fracture process zone at the peak load for representative specimens tested at 10, 15, 20, and 35 mm/min loading rates

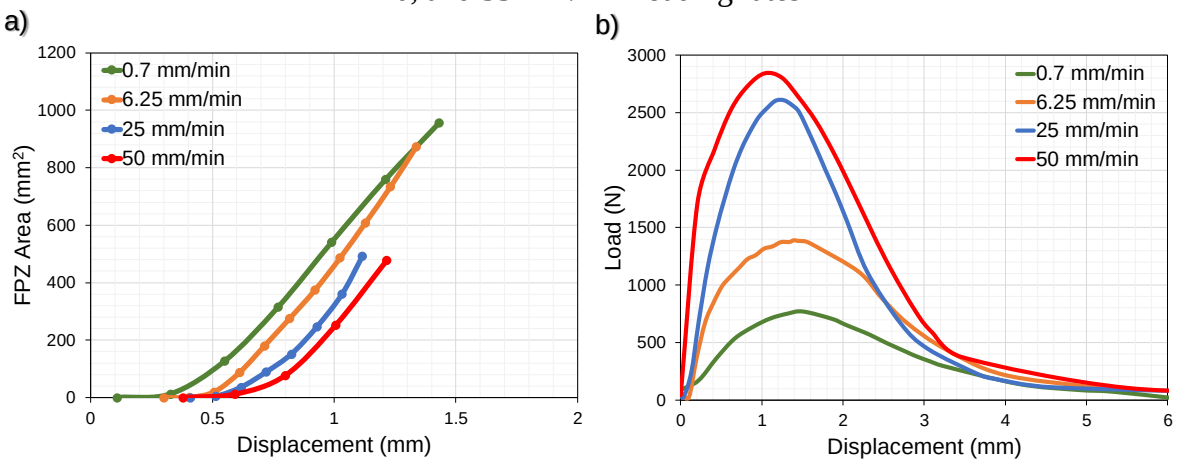

Figure 5.20: a) Fracture process zone area vs displacement a) before the peak load; and b) load vs displacement curves for the loading rate evaluation (for representative specimens)

5.7 Effect of Binder Modification

The impact of binder modification and storage aging is evaluated. The FPZ area was measured using replicates of specimens presented in section 4.5 of this study. Figure 5.21 shows average FPZ area results for AC Mix 1 and Mix 2 tested after 0 days and 60 days of storage. A slight decrease in the FPZ area was observed when the binder grade was modified from PG 64-22 to PG 70-22 SBS under both storage conditions. Also, the average FPZ slightly decreased after 60 days of storage for both AC mixtures. However, the decrease in the FPZ area remained within the range of error (standard deviation) as shown by the error bars. Therefore, a statistical analysis was carried out to evaluate the p-values. The results indicated that the slight change in the FPZ area due to binder modification and shelf aging was not significant. This can be noticeably seen in Figure 5.22 there is no significant difference within the four conditions displayed. The FPZ area change of a variation of approximately 30 mm^2 is within the margin of error for this measurement. Therefore, it can be concluded that there was no noticeable change in the FPZ area.

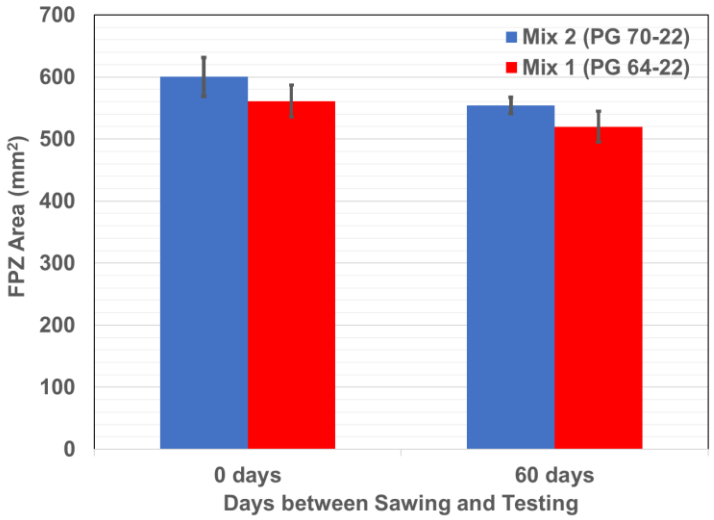

Figure 5.21: Average fracture process zone at the peak load for AC mix 1 and mix 2 at 0 and 60 days storage

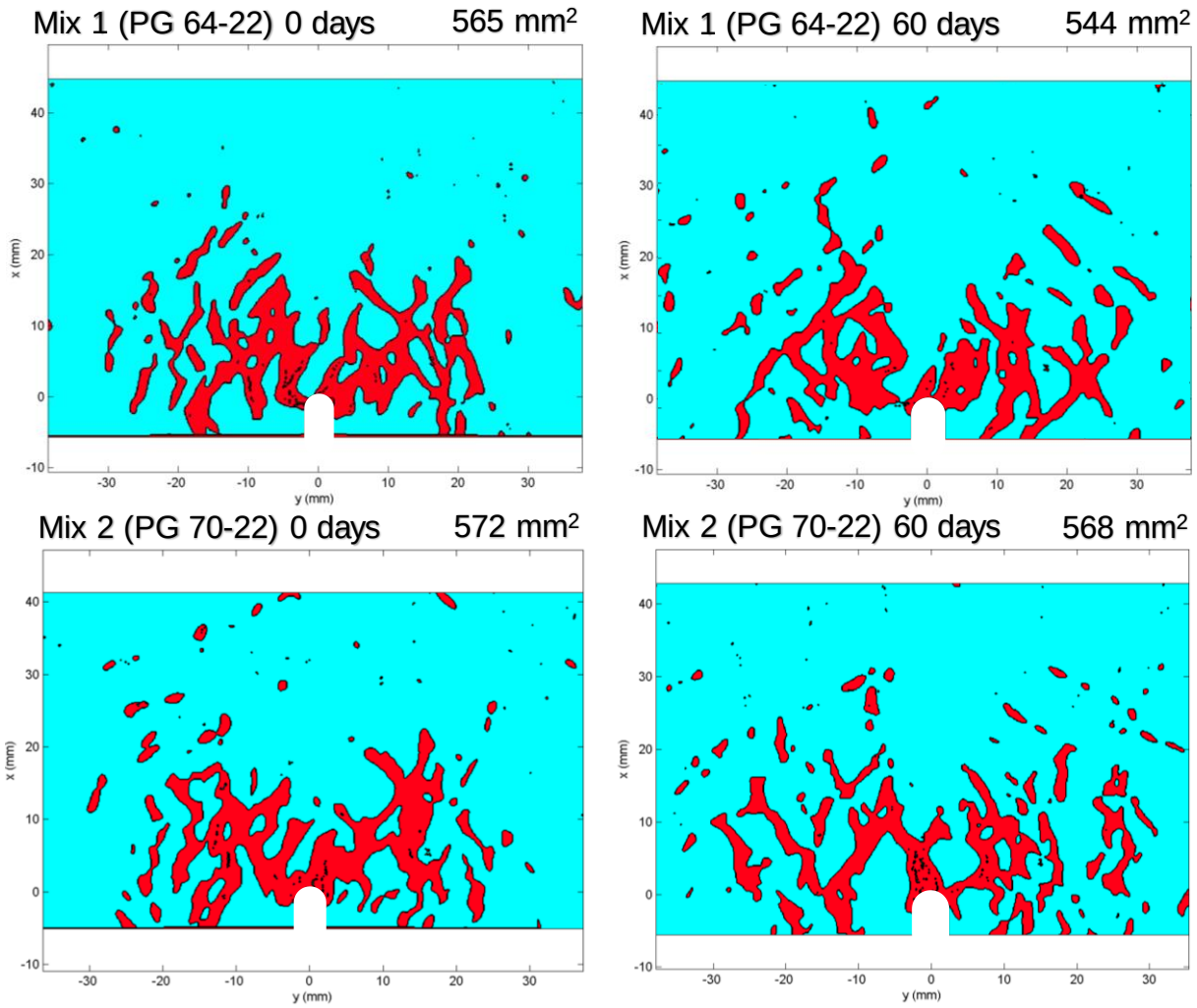

Figure 5.22: Fracture process zone at the peak load for representative specimens of AC mix 1 and mix 2 at 0 and 60 days storage

5.8 Relationship Between FPZ Area and I-FIT Results

The measured FPZ areas were related to the corresponding I-FIT results. The specimen's thickness, air void content, and loading rate were considered. The effect of notch length was not considered, however, because the failure of the long-notched specimens was due to an interaction of compressive and opening tensile strains and not due to the typical mode I opening condition. Also, the binder effect was not considered due to the insignificant statistical variances within the results. Figure 5.23 compares the FPZ area vs the FE, strength, post-peak slope, and FI. A linear

decrement of the FPZ area was observed with the increasing FE and strength. For the post-peak slope, higher FPZ area values coincide with smaller post-peak slopes, but the results did not fit a linear decrement. It appears that there is a no direct correlation between the FPZ area and the FI as shown in Figure 5.23-d.

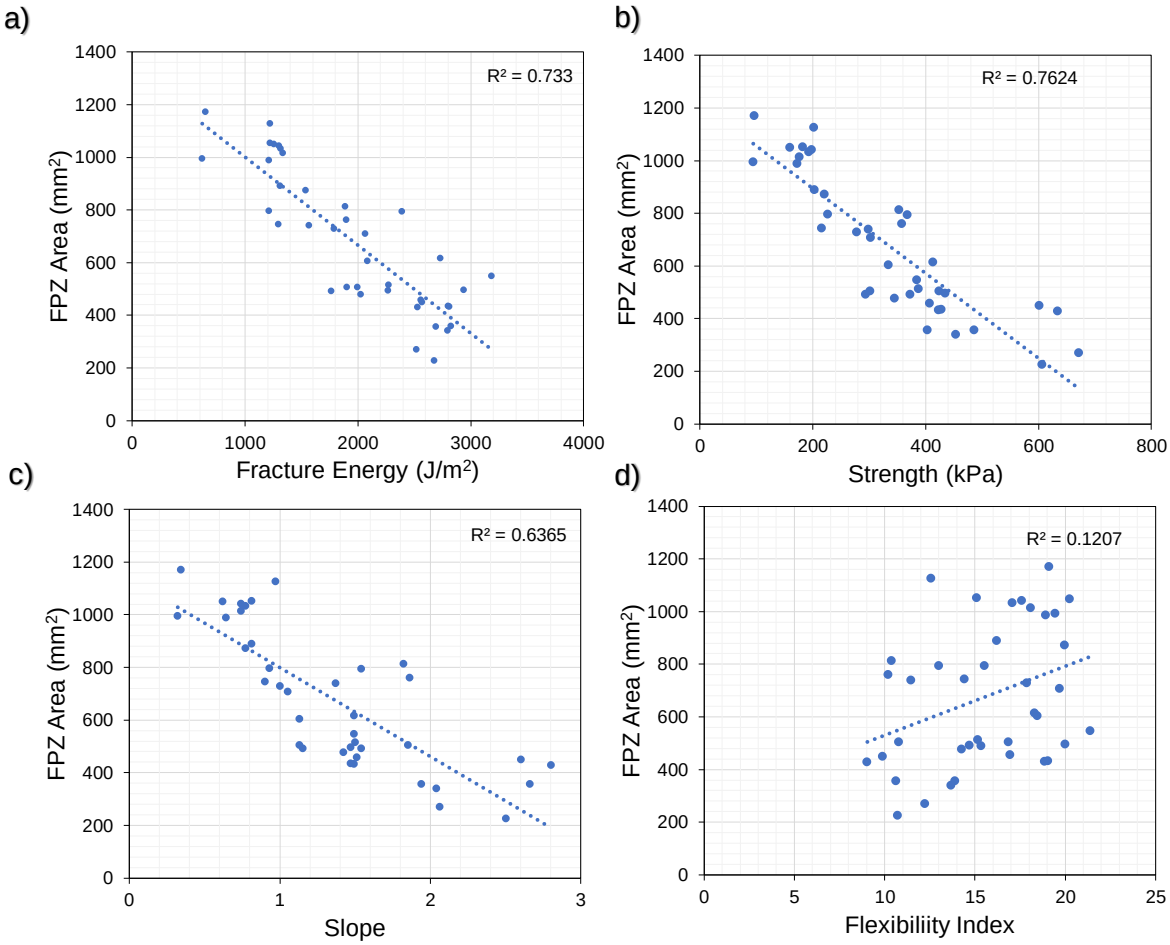

Figure 5.23: Comparison of the fracture process zone area with the I-FIT results: a) FE, b) strength, c) slope and d) FI

5.9 Summary

The FPZ appears to be developed in the mastic matrix of the AC mixture initiating around 70 to 85% of the peak load. The highest strains concentrated in a region close to the notch tip; and decreased with distance away from the crack tip. Thicker specimens exhibit larger FPZ area than

the thinner ones. Similarly, the size of the FPZ increased with air void content. However, the size of the FPZ area decreased with loading rate as AC becomes stiffer. Then, it was observed than a change of the FPZ area affect uniformly all the strain ranges and no redistribution of the strain was observed. Finally, no distinct relationship between the FPZ are and notch length due to the possible interaction of tensile-compressive strain fields.

CHAPTER 6 : SUMMARY, FINDINGS, CONCLUSIONS AND RECOMMENDATIONS

6.1 Summary

The Illinois Flexibility Index Test (I-FIT), AASHTO TP 124-16, has been proven as an effective method for identifying cracking potential within AC mixtures having variable recycled material content. The test is effective, affordable, and easily implementable, rendering results that correlate with field performance. This study evaluated the dependency of the global I-FIT response on the following specimen and testing characteristics: specimen thickness, air void content, notch length, and binder as well as the testing loading rate at the macroscale and microscale. At the macroscale, the study considered variation of FE, strength, post peak slope, and FI with respect to the thickness, loading rate, air void content, notch length and binder characteristics. Correction factors were developed to address the variability caused by specimen thickness, air void content, and notch length. Finally, the microstructure response to test parameters was evaluated by considering the size and strain distribution of the FPZ before failure occurs. To measure the FPZ, images of the surface of the I-FIT specimens were captured during testing to measure the strain field using DIC at a “zoom in” field of view (8 microns/pixel). The size of the FPZ was measured using the strain threshold.

6.2 Findings

The study resulted in the following findings on the effects of thickness, notch length, air voids, loading rate, and binder grade on the global response of the I-FIT (FI, post-peak slope, FE):

- The increased thickness caused an increase in the post-peak slope, resulting in a decrease of the FI. FE and strength were not significantly affected by the thickness variation due to

the normalization to the ligament area. The correction factor for the post-peak slope presented by Al-Qadi et al. (2015) was found to be sufficient in addressing this variation.

- Changes in the air void content from 2 % to 10 % did not significantly affect specimen FE or the strength. However, the post-peak slope decreased as the air void content increased. The correction factor for the post-peak slope proposed by Barry et al. (2016) addressed the variability in the FI. The air voids correction factor for FE was not significant.
- Increasing the notch length from 10 mm to 35 mm resulted in a decrease in the FE, strength, and post-peak slope. Therefore, a correction factor was proposed to correct the FE and post-peak slope results to the standard 15-mm notch length.
- At faster loading rates, the FE, post-peak slope, and strength increased. The data were fit into a power function. The power was used to correct the FE, slope, and strength resulting in a corrected FI. However, as different AC mixes may react differently to changes in the loading rate, this approach needs to be further studied to consider different mixtures compositions.
- According to the mix tested in the study, the use of a polymer modified asphalt binder resulted in higher FE and FI. The specimen sawed and stored for 60 days showed a decrease in the FE and increase in the post-peak slope and, therefore the FI decreased.

The following findings were observed for the effect of the thickness, notch length, air voids, loading rate, and binder to the FPZ:

- The FPZ typically initiated around 70 to 85% of the peak load for I-FIT specimens.
- The FPZ developed in the mastic matrix of the AC mixture around the aggregates because this phase is more compliant than the aggregate phase.

- The largest strains concentrated in the region close to the notch tip; as the distance from the crack tip increased, the strain decreased in the mastic phase.
- The 25-, 30-, and 40-mm-thick I-FIT specimens had larger FPZ area than the 45, 50, 60 mm thick specimens due to mainly higher compliance for specimens with smaller thickness and higher confining stresses at larger thicknesses that restrict deformation of the specimen. There appears to be a transition range of thickness (40-45 mm) where FPZ is no longer affected by changes in the thickness.
- The size of the FPZ increased with larger air void content. Large air void content resulted in more damage to the microstructure of the material, thus allowing micro cracks to expand to larger zones (FPZ).
- The size of the FPZ area decreased with longer notch length. From the results of the thickness, air void content, and loading rate evaluations it was observed that the FPZ decreased as the FE, strength and slope increased. However, the specimens with variable notch lengths had an opposite trend.
- The FPZ was less extended with increased notch length because at longer notches the compressive strain field (not considered in the FPZ definition) at the loading point application contributed a substantial amount of the total deformation experienced by the specimen at failure, while the tensile strain contribution decreased. This gave the impression that the FPZ area under the current definition at failure is lower for specimens with longer notch length.
- At faster loading rates, the size of the FPZ area decreased because AC becomes stiffer at fast load applications due to the viscoelastic nature of the AC mastic matrix.

6.3 Conclusions

Based on the results, the following conclusions are made:

- The thickness, loading rate, notch length and air void content significantly affected the I-FIT results. An increase in the thickness or loading rate resulted in an increase of the post-peak slope without affecting the FE, as a result, the FI decreased. On the other hand, an increase in the notch length or air void content resulted in lower post-peak slope values and higher FI.

- The FPZ area was affected by changes in specimen thickness, loading rate, notch length and air void content. From the results, smaller FPZ area correlated to a decrease in the FE and lower post-peak slope. The results from the notch length evaluation did not follow this trend because, as the notch length increases, because the compressive strains (that were not included in the FPZ definition) contributes a significant portion of the total energy dissipation mechanism at failure.

- The existing correction factors to address the variation due to specimen thickness and air void content were found to be appropriate. A new correction factor to account for the notch length is proposed.

6.4 Recommendations for Future Research

This study aimed to identify changes to the I-FIT properties with respect to the global and microstructural response of the I-FIT specimens and material. However further study should be considered to evaluate the following:

- Additional loading rates, binders, and AC mixtures must be investigated to ensure the validity of the study outcome.
- The storage aging impact considering conditions and other time periods should be considered.
- The correction factor proposed for the notch length should be validated using field cores and plant produced AC mixtures.

REFERENCES

[1] K. R. Hansen, "Asphalt Pavement Industry Survey on Recycled Materials and Warm-Mix Asphalt Usage 2014," National Asphalt Pavement Association, Lanham, MD, 2015.

[2] D. Lippert , H. Ozer, I. Al-Qadi, J. Meister and G. Renshaw, "Illinois Highway Materials Sustainability Efforts of 2014.," Illinois Center for Transportation, Rantoul, Il., 2015.

[3] I. Al-Qadi, S. Carpenter, G. Roberts, H. Ozer, Q. Aurangzeb, M. Elseifi and J. Trepanier, "Determination of Usable Residual Asphalt Binder in RAP.," Illinois Center for Transportation, Rantoul, IL., 2009.

[4] I. Al-Qadi, Q. Aurangzeb and S. Carpenter, "2012," Illinois Center for Transportation, Rantoul, Il., Impact of High RAP Contents on Structural and Performance Properties of Asphalt Mixtures. .

[5] I. Al-Qadi, H. Ozer, J. Lambros, A. EL Khatib, P. Singhvi, T. Khan, J. Rivera-Perez and B. Doll, "Testing Protocols to Ensure Performance of High Asphalt Binder Replacement Mixes Using RAP and RAS," Illinois Center for Transportation, Rantoul, Il., 2015.

[6] H. Ozer, I. Al-Qadi, J. Lambros, A. El-Khatib, P. Singhvi and B. Doll, "Development of the fracture-based flexibility index for asphalt concrete cracking potential using modified semi-circle bending test parameters.," *Construction and Bulding Materials,* vol. 115, pp. 390-401, 2016.

[7] H. Ozer, I. Al-Qadi, P. Singhvi, T. Khan, J. Rivera-Perez and A. El-Khatib, "Fracture Characterization of Asphalt Mixtures with High Recycled Content Using Illinois Semicircular Bending Test Method and Flexibility Index," *Transportation Research Record: Journal of The Transportation Research Board,* vol. 2575, pp. 130-137, 2016.

[8] M. Barry, An Analysis of Impact Factors on the Illinois Flexibility Index Test, Urbana, Il: MS. Thesis University of Illinois at Urbana-Champaign, 2016.

[9] W. Buttlar, B. Hill, R. Kim, M. Kutay, A. Montepara, G. Paulino, C. Petit, I. Pop, R. Roncella, S. Safavizadeh, G. Tebaldi and A. Wargo, "Digital Image Correlation Techniques to Investigate Strain Fields and Cracking Phenomena in Asphalt Materials," *Materials and Structures,* vol. 47, no. 8, 2014.

[10] B. Doll, H. Ozer, J. Rivera-Perez, I. Al-Qadi and J. Lambros, "Investigation of viscoelastic fields in asphalt mixtures using digital image correlation.," *International Journal of Fracture,* pp. 1-20, 2017.

[11] M. Sutton, Orteu and Schreier, Image Correlation for Shape, Motion and Deformation MEasurements: Basic Concepts, Theory and Applications, New York, US: Springer , 2009.

[12] Tex-248-F, "Test Procedure for Overlay Test," Texas Department of Transportation, Austin, TX, 2014.

[13] F. Zhou and T. Scullion, Overlay Tester: A Rapid Performance Related to Crack Resistance Test, College Station, TX.: Texas Transportation Institute, 2005.

[14] A. T. 321-14, "Standard Method of Test for Determining the Fatigue Life of Compacted Asphalt Mixtures Subjected to Repeated Flexural Bending," American Association of State Highway and Transportation Officials, Washington, DC, 2014.

[15] Y. Kim, H. J. Lee and D. Little, "Fatigue characterization of asphalt concrete using viscoelasticity and continuum damage theory," *Journal of the Association of Asphalt Paving Technologists,* vol. 66, pp. 520-569, 1997.

[16] ASTM D7313 − 13, "Standard Test Method for Determining Fracture Energy of Asphalt-Aggregate Mixtures Using the Disk-Shaped Compact Tension Geometry," ASTM International, West Conshohocken, PA , 2013.

[17] M. Wagoner, W. Buttlar and G. Paulino, "Development of a Single-Edge Notched Beam Test for Asphalt Concrete Mixtures," *Journal of Testing and Evaluation,* vol. 33, no. 6, p. 452–460, 2005.

[18] A. T. 105-13, "Determining the Fracture Energy of Asphalt Mixtures Using the Semicircular Bend Geometry," American Association of State Highway and Transportation Officials, Washington DC, 2013.

[19] "AASHTO TP 124-16 Determining the Fracture Potential of Asphalt Mixtures Using Semicircular Bend Geometry (SCB) at Intermediate Temperature," American Association of State Highway and Transportation Officials., Washington, DC., 2016.

[20] B. Mussler, M. Swain and N. Claussen, "Dependence of Fracture Toughness of Alumina on Grain Size and Test Technique," *Journal of the American Ceramic Society,* vol. 65, no. 11, pp. 566-572, 1982.

[21] J. Krager-Kocsis, T. Czigany and E. Moakala, "Thickness dependence of work of fracture parameters of an amorphous copolyester," *Polymers,* vol. 38, no. 18, pp. 4587-4593, 1997.

[22] S. Hashemi, "Plane-stress fracture of polycarbonate films," *Journal of Material Science,* vol. 28, no. 22, 1993.

[23] T. Kusaka, M. Hojo, Y. Mai, T. Kurokawa, T. Nojoma and S. Ochaiai, "Rate dependence of mode I fracture behaviour in carbon-fibre/epoxy composite laminates," *Composites Science and Technology,* vol. 58, no. 3, pp. 591-602, 1998.

[24] Z. Bazant and J. Planas, Fracture and Size effect in concrete and other quasibrittle materials, New York, NY: CRC Press, 1998.

[25] Z. Bazant, "Size effect in blunt fracture: concrete, rock, metal," *ASCE Journal of Engineering Mechanics* , vol. 110, pp. 518-535, 1984.

[26] Z. Bazant and J. Planas, "Generalized size effect equation for quasibrittle materials," *Fatigue Fracture Enginnering Mechanics,* vol. 20, no. 5, pp. 671-687, 1997.

[27] A. Carpinteri, "Decrease of apparent tensile and bending strength with specimen size: two different explanations based on fracture mechanics," *International Journal Solid Structures* , vol. 25, no. 4, pp. 407-429, 1989.

[28] Z. Bazant and M. Kazemi, "Size dependence of concrete fracture energy determined by RILEM work-of-fracture method," *International Journal of Fracture,* vol. 51, no. 2, pp. 121-138, 1991.

[29] M. Wagoner, W. Buttlar and G. Paulino, "Disk-shaped Compact Tension Test for Asphalt," *Society for Experimental MEchanics,* vol. 45, no. 3, pp. 270-277, 2005.

[30] S. Im, Y.-R. Kim and H. Ban, "Rate- and Temperature-Dependent Fracture Characteristics of Asphaltic Paving Mixtures," *Journal of Testing and Evaluation,* vol. 41, no. 2, pp. 1-13, 2013.

[31] Y.-R. Kim and F. Aragao, "Microstructure modeling of rate-dependent fracture behavior in bituminous paving mixtures," *Finite Elements in Analysis and Design,* vol. 63, pp. 23-32, 2013.

[32] G. Nsengiyumva, "Development of Semi-Circular Bending (SCB) Fracture Test for Bituminous Mixtures," University of Nebraska Lincoln, Lincoln, NE, 2015.

[33] A. Braham, W. Buttlar and M. Marasteanu, "Effect of Binder Type, Aggregate, and Mixture Composition on Fracture Energy of Hot-Mix Asphalt in Cold Climates," *Transportation Research Record: Journal of the Transportation Research Board* , vol. 2001, pp. 102-109, 2007.

[34] X. Li, A. Braham, M. Marasteneau, W. Buttlar and R. Williams , "Effect of Factors Affecting Fracture Energy of Asphalt Concrete at Low Temperature," *Road Materials and Pavement Design,* pp. 397-416, 2011.

[35] E. Zegeye, . J.-L. Le, M. Turos and M. Marasteanu, "Investigation of size effect in asphalt mixture fracture testing at low temperature," *Road Materials and Pavement Design,* vol. 13, no. S1, pp. 88-101, 2012.

[36] Z. Wu, L. Mohammad, L. Wang and M. Mull, "Fracture Resistance Characterization of Superpave Mixtures Using the Semi-Circular Bending Test," *Journal of ASTM International,* vol. 2, no. 3, pp. 1-15, 2005.

[37] T. L. Anderson, in *Fracture mechanics: fundamentals and applications*, CRC press, 2005.

[38] X. Li and M. Marasteanu, "The fracture process zone in asphalt mixture at low temperature," *Engineering Fracture Mechanics,* vol. 77, p. 1175–1190, 2010.

[39] K. Zietlow and F. Labuz , "Measurement of the intrinsic process zone in rock using acoustic emission.," *International Journal Rock Mechanics,* vol. 35, no. 3, p. 291–299., 1998.

[40] K. Otsuka and H. Date , "Fracture process zone in concrete tension specimen.," *Journal of Engineering Fracture Mechanics,* vol. 65, pp. 111-131, 2000.

[41] ASTM, "Acoustic Emission STP 505," ASTM international, Philadelphia, 1971.

[42] T. Chu, W. Ranson, M. Sutton and W. Peters, "Applications of Digital Image-Correlation Techniques to Experimental Mechanics," *Experimental Mechanics,* vol. 25, no. 3, 1985.

[43] H. Bruck, S. McNeill, M. Sutton and W. Peters III, "Digital Image Correlation Using Newton-Raphson Method of Partial Differential Correction," *Experimental Mechanics,* vol. 29, no. 3, 1989.

[44] Z. Wu, H. Rong, X. Zheng and W. Dong, "An eexperimental investigation on the FPZ properties in concrete using difital image correlation technique," *Engineering Fracture Mechanics,* vol. 78, 2011.

[45] B. Doll, J. Rivera Perez, H. Ozer, J. Lambros and I. Al-Qadi, "Fracture Process Zone Development in Heterogeneous Asphalt Concrete," *Engineering Fracture Mechanics,* Submitted For Publication 2017.

[46] H. Zelelew and A. Papagiannakis, "Interpreting Asphalt Concrete Creep Behavior throught Non-Newtonian Mastic Rheology.," *Road Materials and Pavement Design,* vol. 13, no. 2, 2012.

[47] B. Hill and W. Buttlar, "Evaluation of polymer modification in asphalt mixtures through digital image correlation and performance space diagrams.," *Construction and Building Materials,* vol. 122, pp. 667-673, 2016 .

[48] E. Romeo, "Measurement and prediction of fundamental tensile failure limits.," Ph.D Dissertation University of Florida, Gainesville, FL, 2008.

[49] Illinois Center for Transportation, "ICT Illinois," University of Illinois, [Online]. Available: https://apps.ict.illinois.edu/software/. [Accessed 22 March 2017].

[50] H. Kim, M. Wagoner and W. Buttlar, "Numerical fracture analysis on the specimen size dependency of asphalt," *Construction and Building Materials,* vol. 23, p. 2112–2120, 2009.

[51] H. Ozer, I. Al-Qadi, J. Lambros, A. El-Khatib, B. Doll and P. Singhvi, "Development of the fracture-based flexibility index for asphalt concrete cracking potential using modified semi-circle bending test parameters.," *Construction and Bulding Materials,* vol. 115, pp. 390-401, 2016.

[52] R. Roque, B. Birgisson, C. Drakos and B. Dietrich, "Development and Field Evaluation of Energy-Based Criteria for Top-Down Cracking Performance of Hot Mix Asphalt.," *Journal of the Association of Asphalt Paving Technologists,* vol. 73, pp. 229-260, 2004.